Al-Azhar Bulletin of Science

Volume 34 | Issue 2 Article 4

2023
Section: Chemistry

SYNTHESIS OF NEW LIGAND-BASED PHOSPHAZO RING AND ITS TRANSITION METAL COMPLEXES AS CANCER INHIBITOR: SPECTROSCOPIC, DFT, ANTIMICROBIAL, AND MOLECULAR DOCKING INVESTIGATIONS

Asmaa A. Hamed
Chemistry Department, Faculty of Science, Al-Azhar University (Girls), Nasr City, Cairo, Egypt, asmaaahmed152@azhar.edu.eg

Ahmed A. El-Sherif
Chemistry Department, Faculty of Science, Cairo University, Giza, Egypt

Carmen M. Sharaby
Chemistry Department, Faculty of Science, Al-Azhar University (Girls), Nasr City, Cairo, Egypt

Yousry A. Ammar
Chemistry Department, Faculty of Science, Al-Azhar University (Boys), Nasr City, Cairo, Egypt

Mona F. Amine
Chemistry Department, Faculty of Science, Al-Azhar University (Girls), Nasr City, Cairo, Egypt

How to Cite This Article

Hamed, Asmaa A.; El-Sherif, Ahmed A.; Sharaby, Carmen M.; Ammar, Yousry A.; and Amine, Mona F. (2023) "SYNTHESIS OF NEW LIGAND-BASED PHOSPHAZO RING AND ITS TRANSITION METAL COMPLEXES AS CANCER INHIBITOR: SPECTROSCOPIC, DFT, ANTIMICROBIAL, AND MOLECULAR DOCKING INVESTIGATIONS," *Al-Azhar Bulletin of Science*: Vol. 34: Iss. 2, Article 4.
DOI: https://doi.org/10.58675/2636-3305.1646

ORIGINAL ARTICLE

Synthesis of a New Ligand-based Phosphazo Ring and its Transition Metal Complexes as a Cancer Inhibitor: Spectroscopic, DFT, Antimicrobial, and Molecular Docking Investigations

Asmaa Ahmed Hamed [a,*], Ahmed Abdou El-Sherif [b], Carmen Mostafa Sharaby [a], Yousry Ahmed Ammar [c], Mona Fakhry Amine [a]

[a] Chemistry Department, Faculty of Science, Al-Azhar University (Girls), Nasr City, Cairo, Egypt
[b] Chemistry Department, Faculty of Science, Cairo University, Giza, Egypt
[c] Chemistry Department, Faculty of Science, Al-Azhar University (Boys), Nasr City, Cairo, Egypt

Abstract

A condensation between 2-sulfonamido pyrimidine and a p-toluidine dimer of cyclodiazadiphosphetidine resulted in the formation of a new ligand, 2,2,4,4-tetrachloro-1,3-di-[p-tolyl]-2,4-di-[N-(pyrimidin-2-yl) benzenesulfonamide]-1,3,2,4-diazadiphosphetidine, (H_2L). We investigated the chemical behavior of the newly prepared ligand by treating it with some chosen metal ions at a stoichiometric ratio of 1:2 (L:M), where M = Fe(III), Fe(II), Cu(II), Zn(II), Cd(II), and Ag(I), to provide colored complexes with accepted yields. Then, we characterized the ligand and related complexes using spectroscopic and analytical techniques. Investigations revealed that the geometrical structure of the complexes was octahedral, except for the silver complex being tetrahedral. From the spectral analyses, we observed that the ligand coordinated with metal ions through the enolic OH of the sulfonamide group and pyrimidine-N of the pyrimidine ring. The molecular geometries have also been optimized using the density functional theory (DFT-B3LYP) methods. In addition, molecular electrostatic potential (MEP) and chemical activity parameters, including chemical hardness, electronegativity, softness, and other parameters have been investigated. We also tested H_2L and its metal complexes for their ability to inhibit the growth of bacterial cells against different types of microorganisms and cancer cells against two different cell lines: MCF-7 and HTC-116. Accordingly, the recently synthesized ligand (H_2L) and its metal complexes exhibited good antimicrobial and antiproliferative actions. Hence, we finally conducted molecular docking of the ligand and its complexes to verify their drug ability.

Keywords: 2-sulfanilamidopyrimidine, Biological, Cyclodiazadiphosphetidine derivative, Metal complexes, Molecular docking

1. Introduction

Two elements in the periodic table generate compounds with the most structural variations, namely, nitrogen and phosphorus [1,2]. In particular, four-membered N_2P_2 ring compounds, with coordination numbers of phosphorus ranging from III to V, have attracted a considerable amount of attention owing to their structural characteristics [3–5]. For example, organophosphorus dimers to coat sheets of bagasse paper with antibacterial surfaces were created by M. El-sakhawy et al. [6]. Their investigations revealed that Gram-positive bacteria (*Bacillus subtilis* and *Staphylococcus aureus*), Gram-negative bacteria (*Pseudomonas aeruginosa*, *Escherichia coli*, and *Proteus vulgaris*), yeasts (*Candida albicans* and *Saccharomyces cerevisiae*), and fungi (*Aspergillus niger*) were all resistant to the antimicrobial activity of the bagasse paper sheets coated with the cyclodiazadiphosphetidine derivative. The chlorine and

Received 25 December 2022; revised 30 January 2023; accepted 2 February 2023.
Available online 23 August 2023

* Corresponding author. 152 Street 9, Mokattam, Cairo 11571, Egypt. Tel: +201149089055
E-mail address: asmaaahmed152@azhar.edu.eg (A.A. Hamed).

https://doi.org/10.58675/2636-3305.1646

phosphorus atoms in the structure of the organophosphorus dimers, including the lone pair of electrons on its nitrogen atoms, were associated with the dimers' capacity to prevent the growth of microbes on the understudied sheets of bagasse paper [6]. Another study by A.M.A. Alaghaz et al. reported treating diazadiphosphetidine of chromene with metal salts, such as Co(II), Ni(II), Cu(II), and Pd(II) [7]. By comparing the synthesized complexes to the ligand, they found that the complexes had strong-to-moderate bactericidal activity [7]. A differently identified compound (cyclodiazadiphosphetidine), featuring a saturated four-membered ring structure, was also found to possess outstanding organic/inorganic characteristics, including various uses such as strong biological activity, the capacity to construct coordination compounds with transition metals, and high substitution sensitivity on P–Cl bonds [8–15].

The aforementioned studies demonstrated the value of phosphorus compounds, thereby accounting for their recognition and use in antioxidants, corrosion-resistant materials, stabilizers (for plastics and oil production), environmentally friendly flame retardants, and agricultural pesticides [16–19]. They also have essential functions in the chemistry of life as structural building blocks for peptides, proteins, and enzymes, generating great interest in studying their functions, primarily in the chemistry of amino acids [20]. However, sulfa medications, such as ampicillin and gentamicin, are among the top choices for chemotherapy and bacterial infection treatments, respectively [21]. Transition metals have been identified as an important family of chemicals owing to their connections to various biological processes [22]. Thus, their ability to form an important class of metal complex-based sulfa medications has recently attracted a considerable amount of attention [23].

Based on the above findings, this research focused on the preparation and characterization of the cyclodiazadiphosphetidine derivative carrying a 2-sulfanilamidopyrimidine moiety, including an investigation of its capacity to create more biologically active metal complex moieties. Then, we performed structural characterizations of the prepared compounds using different physicochemical techniques, after which the H_2L-free ligand and its zinc and silver complexes were molecularly modeled. Finally, the antibacterial and antiproliferative properties and complexes of the synthesized ligand were investigated, followed by molecular docking with all the prepared compounds to verify their drug ability.

2. Materials and methods

2.1. Chemicals, measurements, and computations

Chemicals of high purity used in this study included Para-Toluidine (C_7H_8), phosphorus pentachloride (PCl_5), 2-sulfanilamidopyrimidine ($C_{10}H_9N_4NaO_2S$), ferric chloride hexahydrate ($FeC1_3.6H_2O$), ferrous sulfate heptahydrate ($FeSO_4.7H_2O$), copper(II) chloride dihydrate ($CuC1_2.2H_2O$), zinc(II) chloride anhydrous ($ZnC1_2$), cadmium(II) chloride dihydrate ($CdC1_2.2H_2O$), and silver(I) nitrate ($AgNO_3$) were purchased from Merck or Sigma–Aldrich. Organic solvents, such as ethanol (C_2H_6O), diethyl ether ($(C_2H_5)_2O$), deuterated dimethyl sulfoxide (C_2D_6OS) (DMSO-d_6), and dimethylformamide (C_3H_7NO) (DMF) were purchased from Sigma–Aldrich. Perchloric acid ($HClO_4$), ammonia solution (NH_4OH), ammonium chloride (NH_4Cl), nitric acid (HNO_3), ethylenediaminetetraacetic acid disodium salt ($C_{10}H_{14}N_2Na_2O_8$) (Na_2EDTA), murexide ($C_8H_8N_6O_6$), eriochrome black-T ($C_{20}H_{12}N_3O_7SNa$) (EBT), salicylic acid ($C_7H_6O_3$), and p-chloroaniline (C_6H_6ClN) were all obtained from Merck. The starting 2,2,2,4,4,4-hexachloro-1,3-di-p-tolyl-1,3-diazadiphosphetidine ($C_{14}H_{14}Cl_6N_2P_2$) (**L**) has been described in the literature by Becke-Goehring et al. [24]. The preparations of all solutions in an aqueous medium such as metal solutions, Na_2EDTA, buffer solutions, and indicators were prepared in deionized water. Microanalytical determination of carbon, hydrogen, nitrogen, and sulfur was performed at a microanalytical center at Cairo University. Following a full decomposition of the complexes, the metal contents were assessed by titration against a standard Na_2EDTA solution, except for silver metal which was determined gravimetrically as silver chloride. Then, phosphorus contents were gravimetrically determined [25]. The IR spectra (KBr technique) were carried out using a Perkin–Elmer 437 IR spectrophotometer (400–4000 cm^{-1}). The ^1H and ^{13}C NMR spectra DMSO-*d6* recording was performed using a Bruker FT-400 MHZ spectrophotometer, with TMS as the internal standard. Note that to identify NH peaks in the ^1H NMR spectra of compounds and eliminate the NH signals (proton deuterium exchange), D_2O was added to the NMR sample. A Perkin–Elmer Lambda 3B UV–Vis spectrophotometer was used to record the UV–Vis spectra. Magnetic susceptibilities of the complexes in the solid state were recorded on Sherwood Scientific's Magnetic Susceptibility Balances. The

Klystron-X-band EMX spectrometer (Bruker, Germany) was used to record the electron spin resonance (ESR) spectra for copper complex in the solid state at room temperature. The cavity used here was a standard rectangular ER 4102 cavity with appropriate microwave power (5−10 mW) and 100-kHz magnetic field modulation. With a waveguide, the sample should receive microwave radiation from the klystron. While diphenyl picryl hydrazide (DPPH) was used as the standard material for this investigation, a direct insertion probe was used to record the mass spectra using the Shimadzu-Ge-Ms-QP 100-EX mass spectrometer (Japan) at temperatures ranging from 50 °C to 800 °C. Typically, samples of either solids or solutions are contained in 5-quartz tubes and should have an inner diameter of around 3 or 5 mm [26]. We finally conducted a thermogravimetric analysis using Shimadzu TGA-50H at a flow rate of 20 mL min−1 in a nitrogen atmosphere. The density functional theory (DFT) calculations have been executed to learn more about the synthesized sulfa drug, cyclo-diazadiphosphetidine derivative and its metal complexes [27]. Calculations were performed using the B3LYP/genecp methods [28,29] combined with the basis sets of 6−31-G(d,p) and LanL2DZ [30] for the free ligand and its complexes, respectively, using Gaussian 09 computer program [31]. While the antimicrobial activity was performed using DMF as a solvent and the broth dilution method [32], antitumor activity was performed against two carcinoma cell lines: (MCF-7) and (HCT-116). Finally, the molecular operating environment (MOE) version 2015.10 software was used for molecular docking studies [33]. ChemDraw 18.0 was used to draw the understudied compounds, which were then saved as MDL MOL files; and the crystal structures of the Casp3 protein (PDB ID: 3KJF) were downloaded from the protein data bank.

2.2. Synthesis of the H_2L ligand

For ligand synthesis, 2-sulfanilamidopyrimidine (5 g, 0.02 mol) was added in a dropwise manner for half an hour to a quick-fit flask containing a well-stirred cold solution of 2,2,2,4,4,4-hexachloro-1,3-di-p-tolyl-1,3-diazadiphosphetidine (**L**), (4.85 g, 0.01 mol) in 100-mL acetonitrile. Next, the reaction mixture was placed under reflux for about 3 h, after which the obtained solid product was separated by filtration and then refined by washing with acetonitrile and diethyl ether multiple times, followed by drying under vacuum and over anhydrous $CaCl_2$, thereby retrieving the corresponding substituted diazadiphosphetidine, H_2L.

Yield 55%; yellow solid, m.P = 210 °C. Anal. found (Calcd.) For $C_{34}H_{32}Cl_4N_{10}O_4P_2S_2$ (912.56) (%): C, 43.99(44.75); H, 2.98(3.53); N, 14.13(15.35); Cl, 15.23(15.54); S, 6.48(7.03); P, 6.31(6.79). ^{1}H NMR (500 MHz, DMSO-d_6, δ *in ppm*): 5.12−6.31 (br., 2H, NH); 8.47 (s, H, C−H heterocycle); 6.54−7.62 (d, 4H, aromatic protons) and 2.34 (s, 3H, CH_3). ^{13}C NMR (500 MHz, DMSO-d_6, δ *in ppm*): 21.05 (C_1); 113.05 (C_2); 116.23 (C_3); 125.90 (C_4); 129.82, 130.29 (C_5); 130.59 (C_6); 138.10, 152.95 ($C_{7,8}$); 157.75 (C_9); 158.75 (C_{10}). IR (υ, cm^{-1}): 3355 sharp (NH); 1619 sharp (C]N); 1343 (SO_2)asym; 1069 sharp (SO_2) sym; 1155 sharp (P−N) and 664 sharp (P−Cl). UV−vis. (DMF) (λ_{max}, nm): 273 (phosph (V)azo four-membered rings) and 326 (π-π*) and 352 (n-π*). MS *m*/*z* (%): 912(M, 39%).

2.3. Synthesis of metal complexes

After the H_2L ligand had been successfully prepared, the subsequent focus was on how it interacted with various metal ions: Fe(III), Fe(II), Cu(II), Zn(II), Cd(II), and Ag(I). To this end, a hot solution of H_2L (5 mmol) in 100 mL absolute ethanol was added in a dropwise manner to a hot solution of the aforementioned metal salts (10 mmol) in 50 mL absolute ethanol. For 2 h, the reaction mixture was refluxed. Then, the obtained product was separated, cleaned thoroughly using ethanol and diethyl ether, filtered, and vacuum-dried.

(1) $[(FeCl_3)_2(H_2L)\ (H_2O)_2]$ (**1**), Yield, 20%, Buff solid, m.P > 300 °C. Anal. Found (Calcd.) % for $C_{34}H_{36}Cl_{10}Fe_2N_{10}O_6P_2S_2$ (M.wt, 1272.98): C, 31.90(32.08); H, 2.78(2.85); N, 10.87(11.00); S, 4.89(5.04); Cl, 27.61(27.85); P, 4.59(4.87); Fe, 8.51(8.77). IR (υ, cm^{-1}): 3415 broad (OH); 1581 sharp (C]N); 1334, 1094 sharp (SO_2) asym. and sym. Respectively; 1157 sharp (P−N) and 684 sharp (P−Cl), 840 medium (Coord. H_2O), 546 (M−O), 497 (M−N). UV−vis. (DMF) (λ_{max}, nm): 270 (phosph(V) azo four-membered rings), 335 (π-π*) and 350 (n-π*). μeff (BM): 5.9. Λm (Ω−1 mol−1 cm^2): 3.36.

(2) $[(FeSO_4)_2(H_2L)\ (H_2O)_4]$ (**2**), Yield, 44%, Off white solid, m.P > 300 °C. Anal. Found (Calcd). % for $C_{34}H_{40}Cl_4Fe_2N_{10}O_{16}P_2S_4$ (M.wt, 1287.68): C, 31.20(31.68); H, 3.53(3.10); N, 10.09(10.87); S, 9.21(9.94); Cl, 10.57(11.02) P, 4.21(4.81); Fe, 8.26(8.67). IR (υ, cm^{-1}): 3359 broad (OH); 1584 sharp (C]N); 1335, 1082 sharp (SO_2) asym. and sym. respectively; 1150 sharp (P−N) and 684 sharp (P−Cl), 876 medium (Coord. H_2O), 550 (M−O), 441 (M−N). UV−vis. (DMF) (λ_{max}, nm): 270 (phosph(V) azo four-membered rings), 329

(π-π*) and 380 (n-π*). μeff (BM): 5.2. Λm (Ω^{-1} mol^{-1} cm^2): 1.73.

(3) [$(CuCl_2)_2(H_2L)$ $(H_2O)_4$] (**3**), Yield, 65%, Green solid, m.*P* > 300 °C. Anal. Found (Calcd.) % for $C_{34}H_{40}Cl_8Cu_2N_{10}O_8P_2S_2$ (M.wt, 1253.52): C, 32.19(32.58); H, 2.81(3.22); N, 10.68(11.17); S, 4.97(5.12); Cl, 22.28(22.62); P, 4.57(4.94); Cu, 9.98(10.14). IR (υ, cm^{-1}): 3437 broad (OH); 1584 sharp (C]N); 1330, 1089 sharp (SO_2) asym. and sym. respectively; 1159 sharp (P−N) and 650 sharp (P−Cl), 837 medium (Coord. H_2O), 559 (M−O), 469 (M−N). UV−vis. (DMF) (λ_{max}, nm): 275 (phosph(V) azo four-membered rings), 335 (π-π*) and 345 (n-π*). μeff (BM): 1.9. Λm (Ω^{-1} mol^{-1} cm^2): 2.88.

(4) [$(ZnCl_2)_2(H_2L)$ $(H_2O)_4$] (**4**), Yield, 10%, Pale yellow solid, m.*P* > 300 °C. Anal. Found (Calcd.) % for $C_{34}H_{40}Cl_8Zn_2N_{10}O_8P_2S_2$ (M.wt, 1257.18): C, 32.02(32.48); H, 2.99(3.21); N, 10.98(11.14); S, 5.10(5.10); Cl, 22.29(22.56); P, 4.52(4.93); Zn, 10.29(10.40). IR (υ, cm^{-1}): 3383broad (OH-enolic); 1586sharp (C]N); 1330, 1089 sharp (SO_2) asym. and sym. respectively; 1157 sharp (P−N) and 687 sharp (P−Cl), 847 medium (Coord. H_2O), 550 (M−O), 499 (M−N). ^{1}H NMR: 3.95−5.60 ppm (br., 2H, OH-enolic); 8.48 ppm (s, H, C−H heterocycle); 6.55−7.63 ppm (d, 4H, Aromatic protons) and 2.49 ppm (s, 3H, CH_3); 3.95 ppm (br., 2H, H_2O coordinated water). UV−vis. (DMF) (λ_{max}, nm): 269 (phosph(V)azo four-membered rings), 311 (π-π*) and 350 (n-π*). Λm (Ω^{-1} mol^{-1} cm^2): 3.29.

(5) [$(CdCl_2)_2(H_2L)$ $(H_2O)_4$] (**5**), Yield, 53%, Pale orange solid, m.*P* > 300 °C. Anal. Found (Calcd.) % for $C_{34}H_{40}Cl_8Cd_2N_{10}O_8P_2S_2$ (M.wt, 1351.25): C, 30.19(30.22); H, 2.69(2.98); N, 10.12(10.37); S, 4.32(4.75); Cl, 20.73(20.99); P, 4.12(4.58); Cd, 16.32. IR (υ, cm^{-1}): 3390 broad (OH-enolic); 1580 sharp (C]N); 1320, 1094 sharp (SO_2) asym. and sym. respectively; 1151 sharp (P−N) and 685 sharp (P−Cl), 840 medium (Coord. H_2O), 548 (M−O), 497 (M−N). ^{1}H NMR: 4.20−5.30 ppm (br., 2H, OH-enolic); 8.48 ppm (s, H, C−H heterocycle); 6.56−7.63 ppm (d, 4H, Aromatic protons) and 2.32 ppm (s, 3H, CH_3); 3.45 ppm (br., 2H, H_2O coordinated water). UV−vis. (DMF) (λ_{max}, nm): 270 (phosph(V) azo four-membered rings), 320 (π-π*) and 335 (n-π*). Λm (Ω^{-1} mol^{-1} cm^2): 2.49.

(6) [$(AgNO_3)_2(H_2L)$ $(H_2O)_2$] (**6**), Yield, 45%, Gray solid, m.*P* > 300 °C. Anal. Found (Calcd.) % for $C_{34}H_{36}Cl_4Ag_2N_{12}O_{12}P_2S_2$ (M.wt, 1288.34): C, 31.44(31.70); H, 2.52(2.82); N, 12.74(13.05); S, 4.55(4.98); Cl, 10.92(11.01); P, 4.38(4.81); Ag, 16.25(16.75). IR (υ, cm^{-1}): 3417 broad (OH-enolic); 1581 sharp (C]N); 1334, 1087 sharp (SO_2) asym. and sym. respectively; 1157 sharp (P−N) and 633 sharp (P−Cl), 833 medium (Coord. H_2O), 570 (M−O), 465 (M−N). ^{1}H NMR: 3.45−4.40 ppm (br., 2H, OH-enolic); 8.46 ppm (s, H, C−H heterocycle); 6.52−7.58 ppm (d, 4H, Aromatic protons) and 2.46 ppm (s, 3H, CH_3); 3.45 ppm (br., 2H, H_2O coordinated water). UV−vis. (DMF) (λ_{max}, nm): 267 (phosph(V) azo four-membered rings), 316 (π-π*) and 316 (n-π*). Λm (Ω^{-1} mol^{-1} cm^2): 1.68.

2.4. Biological evaluation

For biological evaluation, the free ligand (H_2L) and its metal complexes were screened against selected microorganisms (Gram-positive [+ve] bacteria: *Bacillus pumilis* [MTCC-2296] and *Streptococcus faecalis* [MTCC -0459], Gram-negative [−ve] bacteria: *E. coli* [ATCC-25955] and *Enterobacter cloacae* [ATCC-23355], yeast: *C. albicans* [ATCC-10231], and fungi: *A. niger* [MTCC-1881]) to assess their potential antibacterial and antifungal activities. The broth dilution method was used with antibiotics penicillin G and ciprofloxacin as the standard antibacterial controls and ketoconazole as the standard yeast and fungi control. Briefly, in the broth dilution method [32], a liquid growth medium containing various doses of the selected antibacterial agent was injected into the understudied microorganisms. After an established incubation period, microbial growth was gauged using spectrophotometric cell counts, where the minimum inhibitory concentration (MIC) value is the minimum chemical amount that prevents microbial growth, given in μg/mL [32]. The H_2L parent ligand and its metal complexes were also screened against human breast and colon cancer cell lines, (MCF-7) and (HCT-116), using doxorubicin, a standard cancer treatment. The biological and potential cytotoxicity of compounds was tested at the Faculty of Medicine, Al-Azhar University.

3. Results and discussion

3.1. Structural elucidation of the synthesized H_2L ligand

We characterized the 2,2,4,4-tetrachloro-1,3-di-[p-tolyl]-2,4-di-[N-(pyrimidin-2-yl) benzenesulfonamide]-1,3,2,4-diazadiphosphetidine H_2L ligand through elemental analyses, mass spectra, IR, UV−Vis, ^{1}H, ^{13}C NMR spectra, and radiographic studies. The results of our elemental analyses (C, H, N, Cl, S, and P) agree with those required by the proposed formula. The mass spectra revealed a molecular ion peak at m/z = 912 (39%) that was

consistent with the molecular formula ($C_{34}H_{32}Cl_4N_{10}O_4P_2S_2$) and a base peak at $m/z = 730$ (100%), compatible with the formula ($C_{24}H_{26}Cl_4N_6O_4P_2S_2$). The ^{1}H NMR spectra of the isolated H_2L-free ligand recorded in DMSO-d_6 at an ambient temperature are shown in Fig. 1. The measured ^{1}H NMR spectrum for the ligand shows a characteristic signal at $\delta = 5.12–6.31$ ppm, corresponding to the resonance of SO_2–NH–, and the exocyclic –NH protons, exchangeable with D_2O [1,34]. Doublet–doublet signal within 6.54–7.62 ppm was attributed to the aromatic protons in the H_2L-free ligand [35]. ^{13}C NMR spectra of the H_2L ligand dissolved in DMSO-*d6* were assessed, Fig. 2. The observed ^{13}C peak at 40 ppm was due to the DMSO. The peak at 21.05 ppm corresponding to the carbon atom of the methyl group (–CH_3) [36] and signals within 116.04–130.59 ppm were characteristic of different aromatic carbon positions [36,37]. While the benzene carbon atoms, attached to the nitrogen atoms of the phosphazo ring, were assigned to the recorded signals at 138.10 and 152.95 ppm, the carbon atoms of two pyrimidine rings were considered to be responsible for the remaining ^{13}C signals, 157.75 and 158.75 ppm [38]. The measured IR spectrum revealed characteristic absorption bands in the IR data from the H_2L ligand at 1155 and 664 cm^{-1}, these bands were characteristic of the υ(P–N) and υ(P–Cl) groups, respectively [39,40]. In comparison to the prepared ligand by Taha R. et al., the IR spectra of the free ligand showed the characteristic stretching vibration bands at 1152 which is characteristic for υ(P–N) [1]. The vibrational bands at 1096 and 1343 cm^{-1} were assigned to $\upsilon(SO_2)_{sym}$ and $\upsilon(SO_2)_{asym}$ of the H_2L-free ligand [41]. Relative to the prepared ligand by Taha R. et al., the ligand exhibits two bands at 1340 and 1088 cm-1 assigned to $\upsilon(SO_2)_{sym}$ and $\upsilon(SO_2)_{asym}$ stretching vibrations for the ligand [1]. The N–H stretching vibration of the sulfonamide group was assigned to the IR band that appeared at 3355 cm^{-1} [3,39], while the presence of the band at 3436 was assigned for υ(NH)

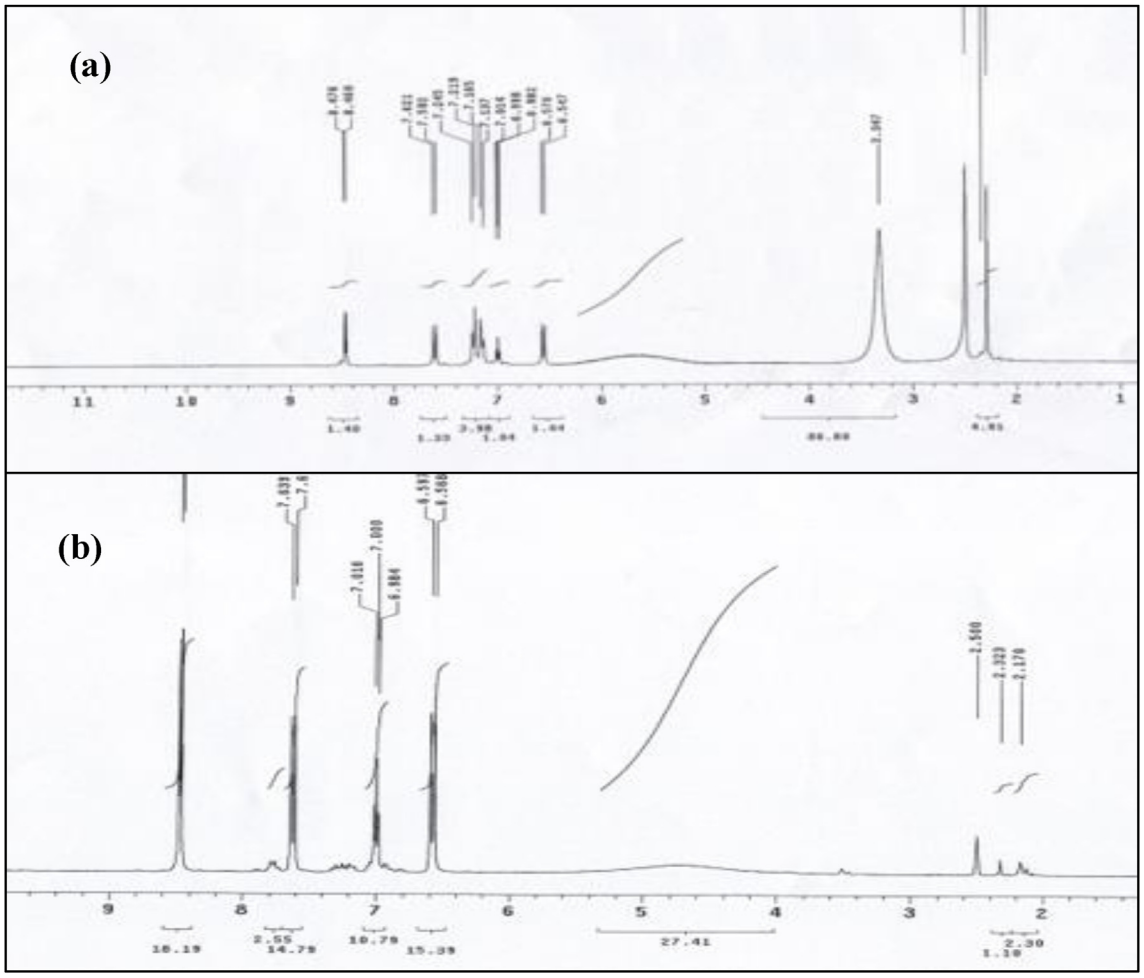

Fig. 1. H NMR spectra of H_2L ligand (a) and its cadmium complex (b).

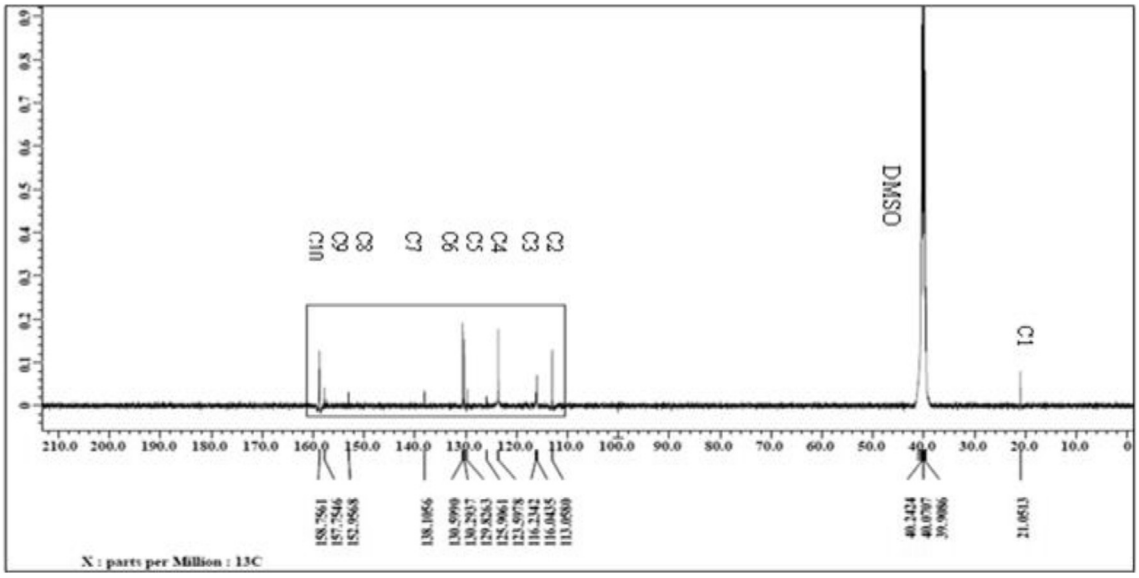

Fig. 2. ^{13}C NMR spectra of the H_2L ligand.

of the ligand prepared by Taha R. et al. [1]. The UV–vis spectra of the H_2L-free ligand in (10^{-3} M), using DMF as a solvent, were also assessed. The spectrum showed an absorption band at 273 nm that was specific to the phosphazo four-membered ring of the dimeric structure [8,42]. According to the study results, we proposed a structure for the newly prepared ligand, as presented in Scheme 1.

3.2. Characterization of the metal complexes

We also subjected the new metal complexes formed between the newly prepared H_2L parent ligand and Fe(III), Fe(II), Cu(II), Zn(II), Cd(II), and Ag(I) ions to elemental analyses, mass spectra, molar conductance, ^1H NMR, IR, UV–Vis, ESR, magnetic studies, radiographic diffraction, and thermal analyses (TGA) to assign chemical structures to the synthesized compounds. Water and most organic solvents formed insoluble complexes, whereas DMF and DMSO formed soluble ones.

(1) While the mass spectrum of the $[(ZnCl_2)_2(H_2L)(H_2O)_4]$ complex **(4)** showed a peak at $m/z = 628$ (38%), corresponding to half of the molecular formula of the complex ($C_{17}H_{20}Cl_4N_5O_4PSZn$), a base peak that appeared at $m/z = 248$ (100%), corresponding to the organic molecular formula ($C_{10}H_8N_4O_2S$), was also observed, including peaks at 79, 93, and 457, due to the ($C_4H_3N_2^+$)/(SO_2NH), ($C_7H_8/C_6H_7N/C_4H_3N_3$), and ($C_{17}H_{17}C_{l2}N_5O_2PS$) moieties, respectively. The mass spectrum of the $[(AgNO_3)_2(H_2L)(H_2O)_2]$ complex (**6**) showed a peak at $m/z = 912$ (13%), which corresponded to its parent ligand molecular formula ($C_{34}H_{32}Cl_4N_{10}O_4P_2S_2$) in this complex. Also, the mass fragmentation pattern showed peaks at $m/z = 77$, 80, 92, 95, 105, 221, 329, and 455, which were thought to be due to $C_6H_5^+$, $C_4H_4N_2/SO_2NH_2$, $C_6H_6N/C7H_8$, $C_4H_5N_3$, C_7H_7N, $C_7H_7Cl_2N_2P/C_6H_5ClNO_2PS$, $C_{13}H_{11}Cl_2N_2PS$, and $C_{17}H_{15}Cl_2N_5O_2PS$ moieties, respectively. Combining these moieties supported the proposed structure of the $[(AgNO_3)_2(H_2L)(H_2O)_2]$ complex.

(2) The molar conductance (ΛM) measurements of all complexes were performed at a concentration of 10^{-3} M using DMF as a solvent. The conductivity values were found within 1.68–3.36 Ω^{-1} cm^2 mol^{-1}, indicating the non-electrolytic nature of the complexes [43,44]. This finding confirms that the anions were inside the coordination sphere of the metal complex.

(3) The ^1H NMR spectra for diamagnetic complexes (**4,5,6**) were recorded in DMSO-d_6, Fig. 1. In the comparison of the characteristic proton signals of $[(ZnCl_2)_2(H_2L)(H_2O)_4]$, $[(CdCl_2)_2(H_2L)(H_2O)_4]$, and $[(AgNO_3)_2(H_2L)(H_2O)_2]$ complexes with those of their H_2L parent ligand, enolization of the secondary amine ($-SO_2NH$) of the H_2L ligand was observed, including a new enolic ($-SO(OH)]N-$). Upon complexation, the enolic proton appeared as a broad signal within $\delta = 3.95–5.60$, 4.20–5.30, and 3.45–4.40 ppm for $[(ZnCl_2)_2(H_2L)(H_2O)_4]$, $[(CdCl_2)_2(H_2L)(H_2O)_4]$, and $[(AgNO_3)_2(H_2L)(H_2O)_2]$ complexes, respectively. These results confirm the involvement of

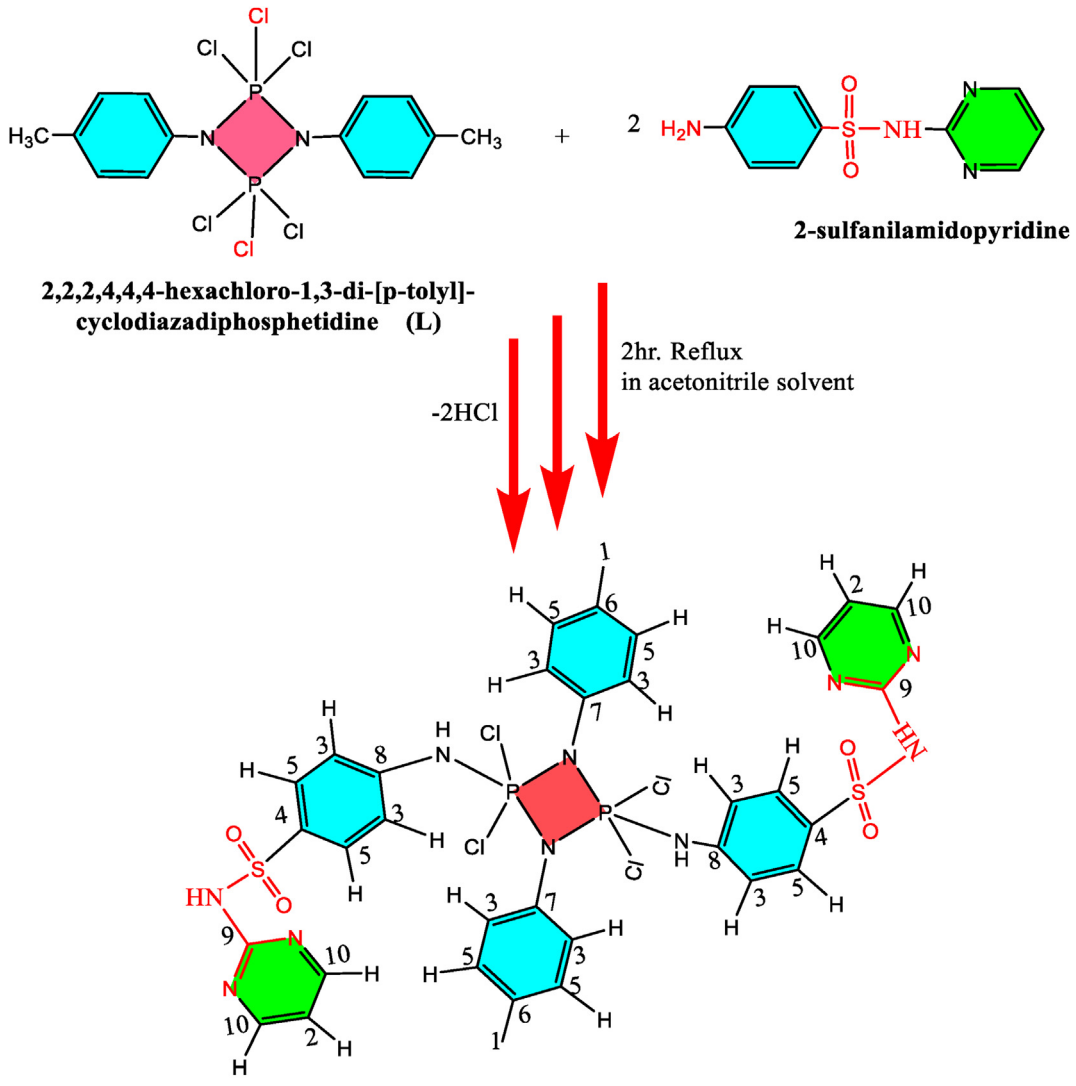

Scheme 1. Suggested structure of newly synthesized H_2L-free ligand.

a sulfonamide group in the complexation [44]. Furthermore, we noticed signals at $\delta = 2.49$, 2.32, and 2.46 ppm for the $[(ZnCl_2)_2(H_2L)\ (H_2O)_4]$, $[(CdCl_2)_2(H_2L)\ (H_2O)_4]$, and $[(AgNO_3)_2(H_2L)\ (H_2O)_2]$ complexes, respectively, which were assigned to the ($-CH_3$) protons [45], including multi-signals of aromatic protons for diamagnetic $[(ZnCl_2)_2(H_2L)\ (H_2O)_4]$, $[(CdCl_2)_2(H_2L)\ (H_2O)_4]$, and $[(AgNO_3)_2(H_2L)\ (H_2O)_2]$ complexes around $\delta = 6.55–7.63$, 6.56–7.63, and 6.52–7.58 ppm, respectively [46]. After complexation, a new signal was observed at $\delta = 3.95$, 3.45, and 3.45 ppm, corresponding to coordinated water molecules for diamagnetic $[(ZnCl_2)_2(H_2L)\ (H_2O)_4]$, $[(CdCl_2)_2(H_2L)\ (H_2O)_4]$, and $[(AgNO_3)_2(H_2L)\ (H_2O)_2]$ complexes, respectively [47,48].

(4) The infrared spectra of the H_2L-free ligand and its metal complexes, Table 1, Fig. 3, were conducted in the range of 4000–400 cm^{-1}, indicating absorption bands due to the respective vibrations. The SO_2 group modes of the H_2L ligand appeared as sharp bands at 1343 cm^{-1} and 1096 cm^{-1} characteristic of the sulfone group $\upsilon(SO_2)_{asym}$ and $\upsilon(SO_2)_{sym}$, respectively [49,50]. In complexes (1–6), the asymmetric and symmetric modes are blueshifted to 1320–1335 cm^{-1} and 1082–1094 cm^{-1}, respectively upon coordination to the transition metals [49,50]. The blueshift of

this SO_2 stretching vibration to lower frequencies may be attributed to the transformation of the sulfonamide (-SO_2NH) to give the enol form (-SO(OH)]N) as a result of complex formation to give a more stable six-membered ring [49,50]. However, the stretching vibration band υ(NH) of the sulfonamide group, found at 3355 cm^{-1} for the H_2L-free ligand, disappeared from the spectra of complexes and new absorption broad bands of the enolic υ(OH) appeared within 3359–3437 cm^{-1}. Therefore, we attributed the disappearance of (NH) and the blue shift of the sulfone group to the enolization of the sulfonamide group [1,41,43], as proposed by the previous ^{1}H NMR data. The enolic (OH) group was formed according to the following tautomerism:

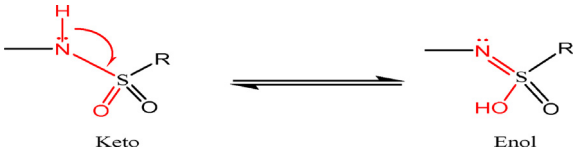

The band due to the pyrimidine moiety, υ(C]N), was shifted to lower frequencies at 1580–1586 cm^{-1} in the spectra of complexes (1–6), suggesting the coordination through the pyrimidine-N atom [[51]. The appearance of a new band in the 833–876 cm^{-1} range is due to out-of-plane bending of coordinated water molecules in the spectra of metal complexes [39,52,53]. These coordinated water molecules were also proven using thermal gravimetric analyses. Also, in the IR spectra of the metal complexes, two additional bands appeared at 546–570 cm^{-1} and 441–499 cm^{-1}, assigned to the υ(M–O) and υ(M–N) stretching vibration, respectively [52,53]. From the above, it is evident that the H_2L ligand coordinated with metal ions through two sites: the enolic OH of the sulfonamide group and pyrimidine-N.

(1) The electronic spectra for the metal complexes in Table 2 were displayed at $l0^{-3}$ M DMF, room temperature, and wavelengths ranging from 200 to 800 nm. Notably, the electronic spectra of the free ligand showed a sharp and intense band at 273 nm that shifted to lower and higher wavelengths in the regions 267–275 nm, corresponding to the phosphazo four-membered ring [1,54]. The band at 326 nm, assigned the π–π* transition for the free ligand shifted to blue or red regions upon complexation within 311–335 nm after complexation [9,55]. In addition, depending on the type of metal ions coordinated to the ligand, the band due to n–π* for the free ligand shifts to lower or higher regions within the 335–380 nm range in the spectra of the complexes [9,55]. Other spectral bands at 415, 424, and 445 nm were also revealed for [$(FeCl_3)_2(H_2L)$ $(H_2O)_2$], [$(FeSO_4)_2(H_2L)$ $(H_2O)_4$], and [$(CuCl_2)_2(H_2L)$ $(H_2O)_4$] respectively, which may be considered ligand-to-metal charge transfer (L-MCT) [41,56]. For the [$(FeCl_3)_2(H_2L)$ $(H_2O)_2$] complex, we observed a *d–d* transition, which displayed absorption bands at 572 and 640 nm (17 482 and 15 625 cm^{-1}) due to the $^6A_{1g} \rightarrow {}^5T_{1g}$ transition in the octahedral geometry [41]. The observed magnetic moment value was at 5.9 BM, confirming an octahedral geometry for the [$(FeCl_3)_2(H_2L)$ $(H_2O)_2$] complex [47]. The [$(FeSO_4)_2(H_2L)$ $(H_2O)_4$] complex had an absorption band at 680 nm (14 705 cm^{-1}), which was assigned to the $^5T_{2g} \rightarrow {}^5E_g$ transition [34]. The observed magnetic moment was 5.2 BM, we suggested a consistent octahedral environment, as evidenced by the octahedral geometry [34]. At the same time, the copper complex produced one main band at 580 nm (17 241 cm^{-1}) due to the $^2E_g \rightarrow {}^2T_{2g}(x^2-y^2)$ transition [57]. The measured magnetic value was 1.9 BM, consistent with an octahedral geometry for the copper complex [46,58]. The UV–vis. spectrum of the [$(ZnCl_2)_2(H_2L)$ $(H_2O)_4$] complex, π–π* and n–π*

Table 1. Observed IR frequencies (4000–400 cm^{-1}) of the H_2L-free ligand and its metal complexes (1–6).

Compound	Assignments								
	υ(NH/ OH-enolic)	υ(C]N) heterocyclic	υ(SO_2) asym.	υ(SO_2) sym.	υ(P–N)	υ(P–Cl)	υ(H_2O) (Coord.)	υ(M–O)	υ(M–N)
H_2L	3355sh	1619sh	1343sh	1096sh	1155sh	664sh	–	–	–
(1)[$(FeCl_3)_2(H_2L)$ $(H_2O)_2$]	3415br	1581sh	1334sh	1094sh	1157sh	684sh	840m	546sh	497m
(2)[$(FeSO_4)_2(H_2L)$ $(H_2O)_4$]	3359br	1584sh	1335sh	1082sh	1150sh	684sh	876m	550sh	441m
(3)[$(CuCl_2)_2(H_2L)$ $(H_2O)_4$]	3437br	1584sh	1330sh	1089sh	1159m	680sh	837m	559sh	469m
(4)[$(ZnCl_2)_2(H_2L)$ $(H_2O)_4$]	3383br	1586sh	1330sh	1089sh	1157m	687sh	847m	550sh	499m
(5)[$(CdCl_2)_2(H_2L)$ $(H_2O)_4$]	3390br	1580sh	1320sh	1094sh	1151m	685sh	840m	548sh	497m
(6)[$(AgNO_3)_2(H_2L)$ $(H_2O)_2$]	3417br	1581sh	1334m	1087m	1157sh	633w	833w	570sh	465w

m, medium; sh, sharp; w, weak.

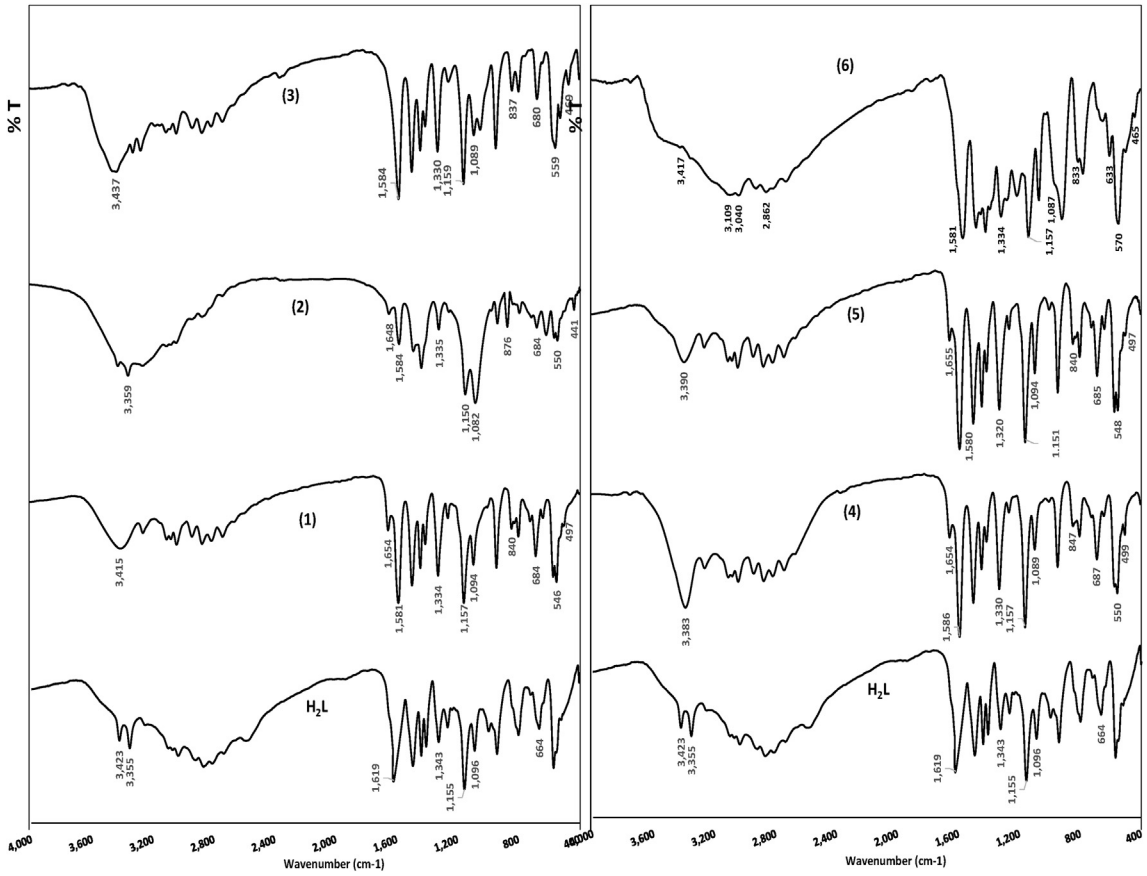

Fig. 3. IR spectra of H_2L ligand and its metal complexes (1–6).

transitions, exhibited blue shift (311 nm) and (350 nm), respectively, as a result of coordination, Table 2 [55]. Also, the UV–vis. spectrum of the $[(CdCl_2)_2(H_2L)\ (H_2O)_4]$ complex, π–π* and n–π* transitions, exhibited blue shift (320 nm) and (335 nm), respectively, upon complexation, Table 2 [55]. Because the $[(ZnCl_2)_2(H_2L)\ (H_2O)_4]$ and $[(CdCl_2)_2(H_2L)\ (H_2O)_4]$ complexes are diamagnetic, no *d–d* transitions were expected for such a filled d^{10} system. An octahedral geometry was still proposed for the $[(ZnCl_2)_2(H_2L)\ (H_2O)_4]$ and $[(CdCl_2)_2(H_2L)\ (H_2O)_4]$ complexes according to the proposed formula [46,59]. The $[(AgNO_3)_2(H_2L)\ (H_2O)_2]$ complex displayed shifting in two absorption bands in the UV–vis. spectrum at (316 nm) and (350 nm) corresponding to π–π* and n–π* transitions, respectively; this shift is as a result of complex formation. From the proposed formula of the diamagnetic $[(AgNO_3)_2(H_2L)\ (H_2O)_2]$ complex, the suggested geometry was a distorted tetrahedral geometry [60,61].

(2) In studying the solid-state $[(CuCl_2)_2(H_2L)\ (H_2O)_4]$ complex, ESR was used to first assess the

Table 2. Electronic spectral data of the H_2L ligand and its metal complexes (1–6).

Number	Ligand/Complex	Absorption bands (nm)										
		Phosphazo ring	π-π*	*n*-π*	*LMCT*	*d–d* transition	μ_{eff}(B.M)	Geometry	$g_{\|\|}$	$g_{\perp}$	$g_{avg.}$	G
	H_2L	273	326	352	–	–	–	–	–	–	–	–
(1)	$[(FeCl_3)_2(H_2L)\ (H_2O)_2]$	270	335	350	415	572, 640	5.9	Octahedral	–	–	–	–
(2)	$[(FeSO_4)_2(H_2L)\ (H_2O)_4]$	270	329	380	424	680	5.2	Octahedral	–	–	–	–
(3)	$[(CuCl_2)_2(H_2L)\ (H_2O)_4]$	275	335	345	445	580	1.9	Octahedral	2.176	2.090	2.133	1.98
(4)	$[(ZnCl_2)_2(H_2L)\ (H_2O)_4]$	269	311	350	d^{10}			Octahedral	–	–	–	–
(5)	$[(CdCl_2)_2(H_2L))\ H_2O)_4]$	270	320	335	d^{10}			Octahedral	–	–	–	–
(6)	$[(AgNO_3)_2(H_2L)\ (H_2O)_2]$	267	316	350	d^{10}			Tetrahedral	–	–	–	–

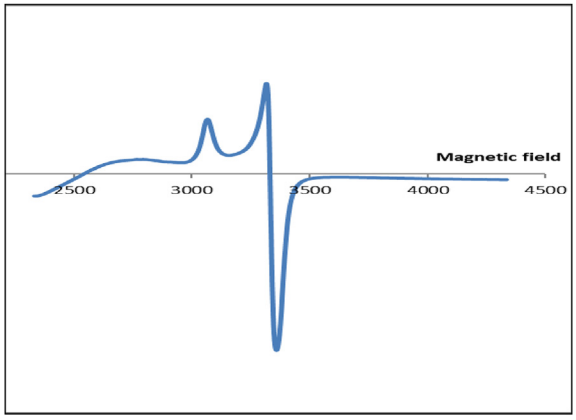

Fig. 4. Electron spin resonance (ESR) spectra of copper (II) complexes (3).

metal ion environment in the paramagnetic ion and the type of its bonding to the nearest neighboring ligand. The powder ESR spectrum of the $[(CuCl_2)_2(H_2L)\ (H_2O)_4]$ complex at room temperature Fig. 4 confirmed an octahedral environment around Cu(II) ion with two g-values ($g_{||} = 2.176$, $g_{\perp} = 2.090$). We also observed the trend $g_{||} > g_{\perp} > g_e$ (2.0023) for this complex, indicating that d_{x2_y2} was the ground state with the d^9 Cu(II) octahedral geometry around the complex's Cu(II) ion [62]. According to Kivelson and Neiman, $g_{||}$ <2.3 indicated covalent characteristics, whereas g|| >2.3 indicated ionic characteristics. This criterion indicates that the $[(CuCl_2)_2(H_2L)\ (H_2O)_4]$ complex under investigation mostly contained covalent metal–ligand bonding. In axial symmetry, the g-values were related by the following formula: $G=(g_{||} - g_e)/(g_{\perp} - g_e)$ where G denotes the exchange interaction parameter, and g_e denotes the free electron g-value (2.0023). According to Hathaway [58], although a considerable exchange contact could exist in solid complexes when G is less than 4, if G is more than 4, the exchange interaction between Cu(II) centers in the solid state becomes insignificant. Based on the distorted octahedral structure, the estimated G parameter for the $[(CuCl_2)_2(H_2L)\ (H_2O)_4]$ complex was 4, showing exchange interactions in the solid copper complexes [63].

(3) Powder radiographic diffraction analysis determined the crystalline size of the synthesized H_2L-free ligand and its metal complexes where their sharp peaks confirmed their crystalline nature Fig. 5. The Debye–Scherrer equation was used to determine the typical crystalline size of the sample, $D = K\lambda/\beta\text{Cos}\ \theta$, where β denotes the full width at half maximum of the characteristic peak; θ, the Bragg diffraction angle for the hkl plane; λ, the wavelength of the radiography source used, which equals 1.54 Å; and K, the constant, which equals 0.94 [64,65]. From the diffraction peaks, the crystal size was calculated as 38 nm for the H_2L-free ligand, 34 nm for the $[(FeCl_3)_2(H_2L)\ (H_2O)_2]$ complex, 17 nm for the $[(FeSO_4)_2(H_2L)\ (H_2O)_4]$ complex, 35 nm for the $[(CuCl_2)_2(H_2L)\ (H_2O)_4]$ complex, 13 nm for the $[(ZnCl_2)_2(H_2L)\ (H_2O)_4]$ complex, 39 nm for the $[(CdCl_2)_2(H_2L)\ (H_2O)_4]$ complex, and 27 nm for the $[(AgNO_3)_2(H_2L)\ (H_2O)_2]$ complex.

(4) The thermal data of metal complexes (2–6) is presented in Table 3. The number of water molecules and whether they were inside the coordination sphere (coordinated) or outside (crystalline) were determined [66].

(a) The TGA curve of the $[(FeSO_4)_2(H_2L)\ (H_2O)_4]$ complex (2) showed four decomposition steps within the temperature range of 34–950 °C. The first step occurred within 34–144 °C, which corresponds to the loss of $3H_2O$ (coordinated) and a mass loss of 3.63% (calculated as 4.19%). However, the second step, with an estimated mass loss of 6.69% (calculated as 7.05%), was within the temperature range of 144–277 °C, which corresponds to one molecule of coordinated water and two molecules of HCl. The third step of decomposition within 277–445 °C corresponded to the removal of one molecule of SO_2 and an organic part C_7H_7N, with an estimated weight loss of 13.31% (calculated as 13.13%). Then, the final step occurred between 277 and 445 °C, corresponding to the removal of one molecule of HCl and an organic part $C_4H_4N_3$, which accounted for an estimated weight loss of 9.11% (calculated as 10.12%). This

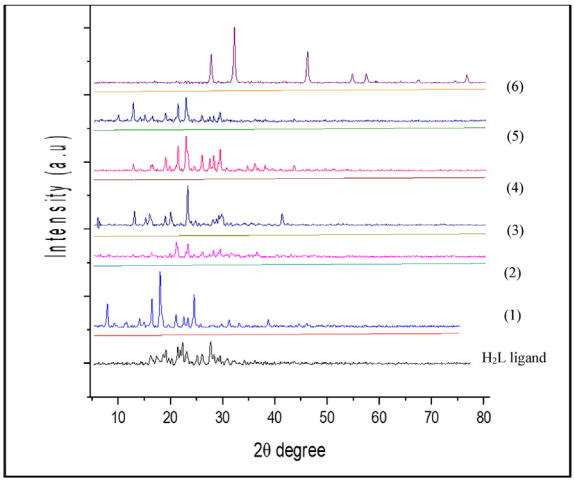

Fig. 5. Radiography powder diffractogram of H_2L-free ligand and its metal complexes.

Table 3. Thermogravimetric results (TG) of H_2L metal complexes (2,3,4,5,6).

Number	Temperature Range (°C)	*n**	Loss in weight estimation/(calc.)%		Assignment	Metallic residue
			Mass loss	Total mass loss		
(2)	34–144 144–277 277–445 445–950	4	3.63 (4.16) 6.69 (7.05) 13.31 (13.13) 9.11 (10.12)	36.90 (36.82)	-Loss of 3Coord.H_2O -Loss of H_2O and 2HCl -Loss of C_7H_7N and SO_2 -Loss of $C_4H_4N_3$ and HCl Leaving $C_{23}H_{18}N_6ClO_8P_2S_3$	2FeO
(3)	32–130 130–206 206–419 419–666	4	5.38 (5.74) 4.94 (4.38) 34.02 (34.14) 32.86 (32.54)	77.20(76.80)	-Loss of 4Coord.H_2O -Loss of HCN and N_2 -Loss of C_7H_7NP and 8HCl -Loss of C_6H_5SO, $C_4H_4N_3SO$ and $C_{10}H_7N$ Leaving C_6N_2P	2CuO
(4)	163–412 412–556	2	25.54 (26.53) 11.28 (10.37)	36.82 (36.90)	- Loss of 4Coord.H_2O & $C_{10}H_9N_4SO_2$ -Loss of HCl and C_7H_7N Leaving $C_{17}H_{15}Cl_7N_5O_4P_2S$	2ZnO
(5)	30–161 161–219 219–423 423–554 554–782	5	1.82 (1.33) 4.53 (3.99) 40.36 (40.57) 12.28 (12.76) 21.49 (22.27)	80.48(80.92)	-Loss of Coord.H_2O -Loss of 3Coord.H_2O -Loss of 7HCl and C_7H_7N and $2C_4H_4N_3$ -Loss of C_7H_7NP and HCl -Loss of $C_{12}H_2N_2O_2PS_2$	2CdO
(6)	23–253 253–378 378–545 545–715	4	4.34 (4.88) 13.10 (13.81) 7.34 (7.29) 27.64 (27.47)	52.45 (53.45)	-Loss of 2 Coord.H_2O and HCN - Loss of C_7H_7N and 2HCl - Loss of $C_4H_4N_3$ - Loss of C_7H_7N and $C_4H_4N_3SO$ and C_6H_5NO Leaving $rC_5H_2N_2O_8P_2S$	

n* = the number of decomposition steps.

final step leaves $C_{23}H_{18}N_6ClO_8P_2S_3$ and 2FeO as metallic residues. Overall, the weight losses amounted to 32.74% (calculated as 34.49%).

(b) However, the TGA curve of the $[(CuCl_2)_2(H_2L)(H_2O)_4]$ complex **(3)** also showed four decomposition steps but within the temperature range of 32 °C–666 °C. The first step occurred within the temperature range of 32–130 °C, which corresponds to the loss of $4H_2O$ (coordinated) and a mass loss of 5.38% (calculated as 5.74%). Then, the second step, with an estimated mass loss of 4.94% (calculated as 4.30%), was within 130–206 °C, which corresponds to the decomposition of one molecule of HCN and N_2. The third step, with an estimated mass loss of 34.02% (calculated as 34.14%), was within 206–419 °C, which corresponds to the loss of 8HCl and an organic part, C_7H_7NP. Finally, the fourth step, at a temperature range of 419–666 °C, showed an estimated mass loss of 32.86% (calculated as 32.62%) that we attributed to the loss of two organic parts of the ligands C_6H_5SO, $C_4H_4N_3SO$, and $C_{10}H_7N$. These steps leave C_6N_2P and 2CuO as metallic residues, resulting in an overall weight loss of 77.20% (calculated as 76.80%).

(c) Alternately, thermograms of the $[(ZnCl_2)_2(H_2L)(H_2O)_4]$ complex **(4)** exhibited a two-step decomposition. The first step involves an estimated weight loss of 26.53% (calculated as 25.54%), which corresponds to the removal of four water molecules of coordination and an organic part $C_{10}H_9N_4O_2S$ within a temperature range of 27–405 °C. Then, the last step (408–556 °C), with an estimated mass loss of 10.37% (calculated as 11.28%) corresponds to the loss of an organic part of C_7H_7N and one molecule of HCl. This step leaves $C_{17}H_{15}N_5Cl_7P_2S$ and 2ZnO as metallic residues, with the overall weight loss amounting to 36.9% (calculated value, 36.82%).

(d) The thermal decomposition of the $[(CdCl_2)_2(H_2L)(H_2O)_4]$ complex **(5)** shows a decomposition pattern as follows: the first step within a temperature range of 30–161 °C represents the loss of one molecule of coordinated water, coupled with a mass loss of 1.82% (calculated as 1.33%). The second step was with an estimated mass loss of 4.53% (calculated as 3.99%) within 161–219 °C, corresponding to the loss of $3H_2O$ of coordination. Then, the third step, with an estimated mass loss of 40.36% (calculated as 40.57%), was within the temperature range of 219–423 °C, corresponding to the loss of 7HCl and organic parts of the ligand C_7H_7N and $2C_4H_4N_3$. The fourth step 423–554 °C, with an estimated mass loss of 12.28% (calculated as 12.76%), was attributed to the loss of one molecule of HCl and an organic part of the ligand ($C_8H_{10}N_2$). Finally, the last step at 554–782 °C, with an estimated weight loss of 21.49% (calculated as 22.27%), corresponded to the removal of an organic part, C_7H_7NP, leaving $C_{12}H_2N_2O_2PS_2$ and 2CdO as a metallic residue. Consequently, the overall weight amounted to 80.48% (calculated as 80.92%).

(e) The thermogram of the $[(AgNO_3)_2(H_2L)(H_2O)_2]$ complex **(6)** exhibited a four-step decomposition process. The first step involved an estimated

Table 4. Thermodynamic data of the thermal decomposition of H_2L metal complexes (2,3,4,5,6).

Comp. Number	Decomposition Temp	Tp/K	R^2		Δ E* (J mol^{-1})		A (S^{-1})		Δ S* (K^{-1} mol^{-1})		Δ H* (J mol^{-1})		Δ G* (J mol^{-1})	
			HM	CR	HM	CR	HM	CR	HM	CR	HM	CR	HM	CR
(2)	34–144	428	0.93	−0.78	527	61531	1.66×10^3	1.06×10^9	−208	−319	−3450	7963	175173	76099
	144–277	579	0.92	−0.89	292	37539	3×10^2	6.2×10^5	−195	−247	−3726	42520	167047	80774
	277–445	625	0.99	−0.99	175	48806	4.1×10^2	1.3×10^6	−186	−273	−5691	34938	199179	99262
	445–950	885	0.94	−0.90	98	57633	1.3×10^2	1.3×10^7	−172	−293	−7544	21090	263751	153751
(3)			HM	CR	HM	CR	HM	CR	HM	CR	HM	CR	HM	CR
	32–130	354	0.93	−0.93	597	69856	7.7×10^3	1.4×10^9	−223	−323	−2351	66907	181743	76769
	130–206	441	0.98	−0.92	239	38995	4.1×10^2	3.1×10^5	−197	−252	−3434	35321	146692	83584
	206–419	585	0.98	−0.97	132	34630	3.5×10^2	2.3×10^7	−193	−285	−4743	29755	197259	108559
	419–666	816	0.95	−0.89	92	45440	1.2×10^2	4.7×10^7	−181	−288	−6697	38651	274286	141681
			HM	CR	HM	CR	HM	CR	HM	CR	HM	CR	HM	CR
(4)	163–412	456	0.95	−0.93	200	32742	8.6×10^2	3.8×10^7	−200	−283	−4595	28947	17685	111942
	412–556	438	0.99	−0.98	83	40463	1.4×10^2	5.5×10^7	−199	−295	−6565	36815	27427	148293
(5)			HM	CR	HM	CR	HM	CR	HM	CR	HM	CR	HM	CR
	30–161	371	0.85	−0.84	251	30041	1.09×10^3	9.9×10^5	−206	−263	−2842	26948	124793	73928
	161–219	482	0.92	−0.89	192	36539	3.9×10^2	6.6×10^5	−195	−257	−3826	32520	157047	90774
	219–423	585	0.99	−0.99	176	49806	5.1×10^2	1.6×10^6	−196	−263	−4691	44938	199179	110262
	423–554	786	0.94	−0.90	99	47633	1.2×10^2	2.3×10^7	−182	−283	−6444	41090	263751	263751
	554–782	899	0.99	−0.98	130	89857	1.9×10^2	4.2×10^5	−184	−248	−7353	82373	306214	158820
(6)			HM	CR	HM	CR	HM	CR	HM	CR	HM	CR	HM	CR
	23–253	411	0.96	−0.96	146	18182	9×10^2	8.5×10^7	−204	−299	−3277	14758	80886	137979
	253–378	589	0.99	−0.98	176	50751	4.4×10^2	1.3×10^6	−195	−261	−4726	45849	110280	200194
	378–545	734	0.95	−0.84	52	15622	7.3×10^1	9×10^8	−178	−314	−6060	9509	125072	240356
	545–715	903	0.96	−0.93	92	58727	1.9×10^2	3.9×10^7	−184	−286	−7423	51211	159392	309899

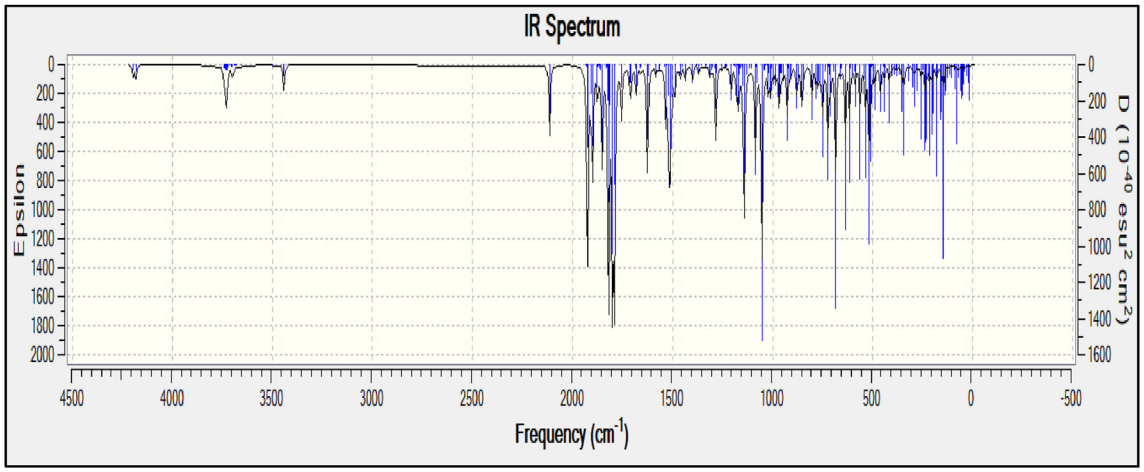

Fig. 6. Theoretical IR spectrum of the H_2L-free ligand.

weight loss of 4.34% (calculated as 4.88%), corresponding to the removal of two water molecules of coordination within the temperature range of 23–253 °C. Then, the second step, with an estimated mass loss of 13.10% (calculated as 13.81%), was within the temperature range of 253–378 °C, which corresponds to the loss of 2HCl and an organic part of the ligand C_7H_7N. The third step, with an estimated mass loss of 7.34% (calculated as 7.29%), was within the temperature range of 378–545 °C, corresponding to the loss of an organic part $C_4H_4N_3$, and the last step was in the temperature range of 545–715 °C, with an estimated mass loss of 27.64% (calculated as 27.47%), corresponding to the loss of different organic ligand parts: C_7H_7N, C_6H_5NO, and $C_4H_4N_3SO$. This step leaves $C_5H_2N_2O_8P_2S$ and 2AgCl as metallic residues, causing the overall weight loss amount to be 52.45% (calculated as 53.45%).

(5) The Coats–Redfern and Horowitz Metzger [67] relation is used to graphically analyze the thermodynamic activation parameters of complicated decomposition processes, including the activation energy (E*), enthalpy (H*), entropy (S*), and Gibbs free energy change (G*) [68]. Therefore, we calculated the entropy of activation (Δ S*), enthalpy of activation (Δ H*), and free energy change of activation (Δ G*) using the Excel computer program for complexes, Table 4 sums up this information. While the high values for (E*) indicated that these complexes were thermally stable, (Δ S*) had a negative value in the complexes, suggesting that the decomposition reactions proceeded at a lower rate than the normal ones. The (Δ G*) values adequately increased for the frequent decomposition steps due to increasing TΔ S* values [69], the (Δ H*) values and their signs depended on the

Table 5. Some B3LYP Structural parameters for the H_2L-free ligand using the 6-31G (d,p) basis set.

Structural parameters	
Bond lengths (Å)	H_2L ligand
$P_1–N_{23}P_2–N_{24}$	1.682
$P_1–N_{24}P_2–N_{23}$	1.850
$P_1–N_{33}P_2–N_{36}$	1.759
$P_1–Cl_{39}P_2–Cl_{34}$	2.130
$P_1–Cl_{38}P_2–Cl_{35}$	2.108
$N_{33}–H_{48}]N_{36}–H_{37}$ (Exocyclic NH)	1.011
$N_{53}–H_{88}N_{69}–H_{87}$ (Sulfonamide NH)	1.014
$C_4–N_{24}C_{16}–N_{23}$	1.426
C]C (benzene ring)	1.391
C–H (benzene ring)	1.085
$C_{43}–N_{33}C_{72}–N_{36}$	1.394
$C_{44}–S_{52}C_{71}–S_{70}$	1.787
$S_{52}]O_{54}S_{70}]O_{75}$	1.464
$S_{52}]N_{53}S_{70}]N_{69}$	1.710
$C_{82}–N_{53}C_{65}–N_{69}$	1.389
$C_{65}–N_{61}C_{82}N_{79}$ (pyrimidine ring)	1.339
C]C (pyrimidine ring)	1.394
C–H (pyrimidine ring)	1.088
Bond angles °	
$P_1–N_{23}– P_4P_1–N_{24}– P_2$	100.6
$N_{23}–P_1– N_{24}N_{23}–P_2– N_{24}$	79.6
$Cl_{38}–P_1– Cl_{39}Cl_{34}–P_2– Cl_{35}$	110.9
$P_1–N_{33}– C_{34}P_2–N_{36}– C_{72}$	130.8
$P_1–N_{33}– H_{48}P_2–N_{36}– H_{37}$	111.3
$C_{41}–C_{45}–N_{33}C_{67}–C_{72}–N_{36}$	121.3
$C_{29}– N_{62}–H_{64}C_{32}– N_6–H_{63}$	113
$C_{41}–C_{43}–C_{45}C_{67}–C_{72}–C_{74}$	118.5
$C_{42}–C_{44}–S_{52}C_{66}–C_{71}–S_{70}$	119.5
$O_{51}]S_{52}]O_{54}O_{68}]S_{70}]O_{75}$	121.6
$O_{51}]S_{52}–N_{53}O_{68}]S_{70}–N_{69}$	109.9
$N_{53}–C_{82}–N_{84}N_{69}–C_{65}–N_{61}$	118
N–C–N (pyrimidine ring)	127
Dihedral	
$N_{23}– P_1–N_{24}–P_2$	0.00
$N_{33}– P_1–N_{24}–P_2$	129.9
$N_{36}– P_2–N_{23}–P_1$	157
$P_1–N_{33}–H–C_{43}$	159
$P_2–N_{36}–H–C_{72}$	161
$S_{52}– N_{53}–C_{82}–N_{84}S_{70}– N_{69}–C_{65}–N_{61}$	24.7
Pyrimidine ring	0.14
Benzene ring	0.3–0.7

Table 6. Selected structural parameters and quantum chemical descriptors of the H_2L-free ligand and its $[(ZnCl_2)_2(H_2L)\ (H_2O)_4]$, $[(AgNO_3)_2(H_2L)\ (H_2O)_2]$ complexes (4,6).

Bond lengths (Å)	H_2L	$[(ZnCl_2)_2(H_2L)\ (H_2O)_4]$ complex	$[(AgNO_3)_2(H_2L)\ (H_2O)_2]$ complex
C–N $_{pyrimidine}$	1.339	1.359	1.363
C–N $_{sulfonamide}$	1.387	1.402	1.389
N–S $_{sulfonamide}$	1.713	1.550	1.551
S–O $_{sulfonamide}$	1.460	1.647	1.652
M–O $_{sulfonamide}$	–	2.649	2.756
M–O $_{(H2O)}$	–	2.240	2.239
M–N $_{pyrimidine}$	–	2.257	2.256
Zn–Cl/Ag–ONO_2	–	2.353	2.338
Bond angles (°)	H_2L	$[(ZnCl_2)_2(H_2L)\ (H_2O)_4]$ complex	$[(AgNO_3)_2(H_2L)\ (H_2O)_2]$ complex
O(81)-Zn(82)-N(88)/O(74)-Ag(100)-N(57)	–	90	83.3
O(85)-Zn(82)-N(88)/O(49)-Ag(100)-N(57)	–	75.5	76.9
O(81)-Zn(82)-O(85)/O(74)Ag(100)–O(49)	–	74	107.5
O(81)-Zn(82)-Cl(80)/O(74)-Ag(100)-O(73)	–	82.9	124
N(88)-Zn(82)-Cl(80)/N(88)-Ag(100)-O(73)	–	101.2	92
Calculated quantum chemical parameters	H_2L	$[(ZnCl_2)_2(H_2L)\ (H_2O)_4]$ complex	$[(AgNO_3)_2(H_2L)\ (H_2O)_2]$ complex
E (a.u)	−5481.91	−7761.04	−6487
Dipole moment (Debye)	3.89	10.46	22.80
E_{HOMO} (ev)	−6.22	−6.54	−5.11
E_{LUMO} (ev)	−2.12	−2.37	−2.75
$\Delta E = (E_{LUMO} - E_{HOMO})$ (ev)	4.10	4.17	2.35
$X = -(E_{HOMO} + E_{LUMO})/2$ (ev)	4.17	4.45	3.93
$\eta = (E_{LUMO} - E_{HOMO})/2$ (ev)	2.05	2.085	1.18
$\sigma = 1/\eta\ (ev)^{-1}$	0.487	0.479	0.847
$Pi = -X$ (ev)	−4.17	−4.45	−3.93
$S = 1/2\eta\ (ev)^{-1}$	0.243	0.239	0.423
$\omega = Pi^2/2\eta$ (ev)	4.24	4.74	6.54
$\Delta N_{max} = -Pi/\eta$	2.03	2.134	3.33

complexes' heat of formation and their solvent effects, which were positive values in all cases, showing that the reaction was endothermic [70].

3.3. Theoretical calculations

Next, using the Gaussian09 program [31], we performed the fully geometrical optimization to obtain structural details about the prepared H_2L-free ligand and its $[(ZnCl_2)_2(H_2L)\ (H_2O)_4]$, $[(AgNO_3)_2(H_2L)\ (H_2O)_2]$ complexes, after which calculations were performed (DFT) using the B3LYP/genecp method. The geometry optimization was carried out using the B3LYP/genecp method and the 6–31-G(d,p) basis set for the H_2L-free ligand, implementing the Gaussian 09 program. In

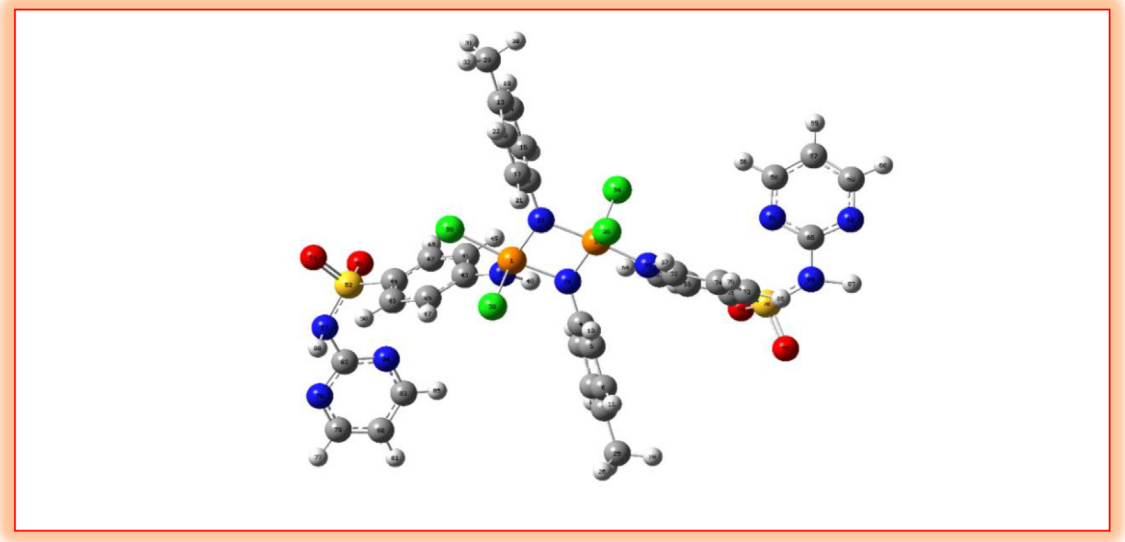

Fig. 7. Optimized structure of the newly synthesized H_2L-free ligand.

case of $[(ZnCl_2)_2(H_2L)\ (H_2O)_4]$ and $[(AgNO_3)_2(H_2L)\ (H_2O)_2]$ metal complexes, LanL2DZ basis set was used. After geometrical optimization, frequency calculations for the H_2L parent ligand had been simulated using a Gaussian computer program showing all positive frequencies (no imaginary frequency modes were obtained), indicating true minimum geometry on the potential energy surface Fig. 6. The bond lengths/angles, dihedral angles, and selected structural parameters are presented in Tables 5 and 6. It has been found that the sum of calculated internal angles in the $(P-N)_2$ four-membered ring was 360° and the dihedral angle is 0.00. This means that the phosphazo four-membered ring was planar, which perfectly agrees with the observed experimental parameter values of the radiography single-crystal reported studies of the $(P-N)_2$ four-membered ring for different compounds [71,72]. The benzene ring formed at a ~90° dihedral angle with the phosphazo ring, indicated that it was perpendicular to the latter; the phosphorus atom exhibited a distorted trigonal

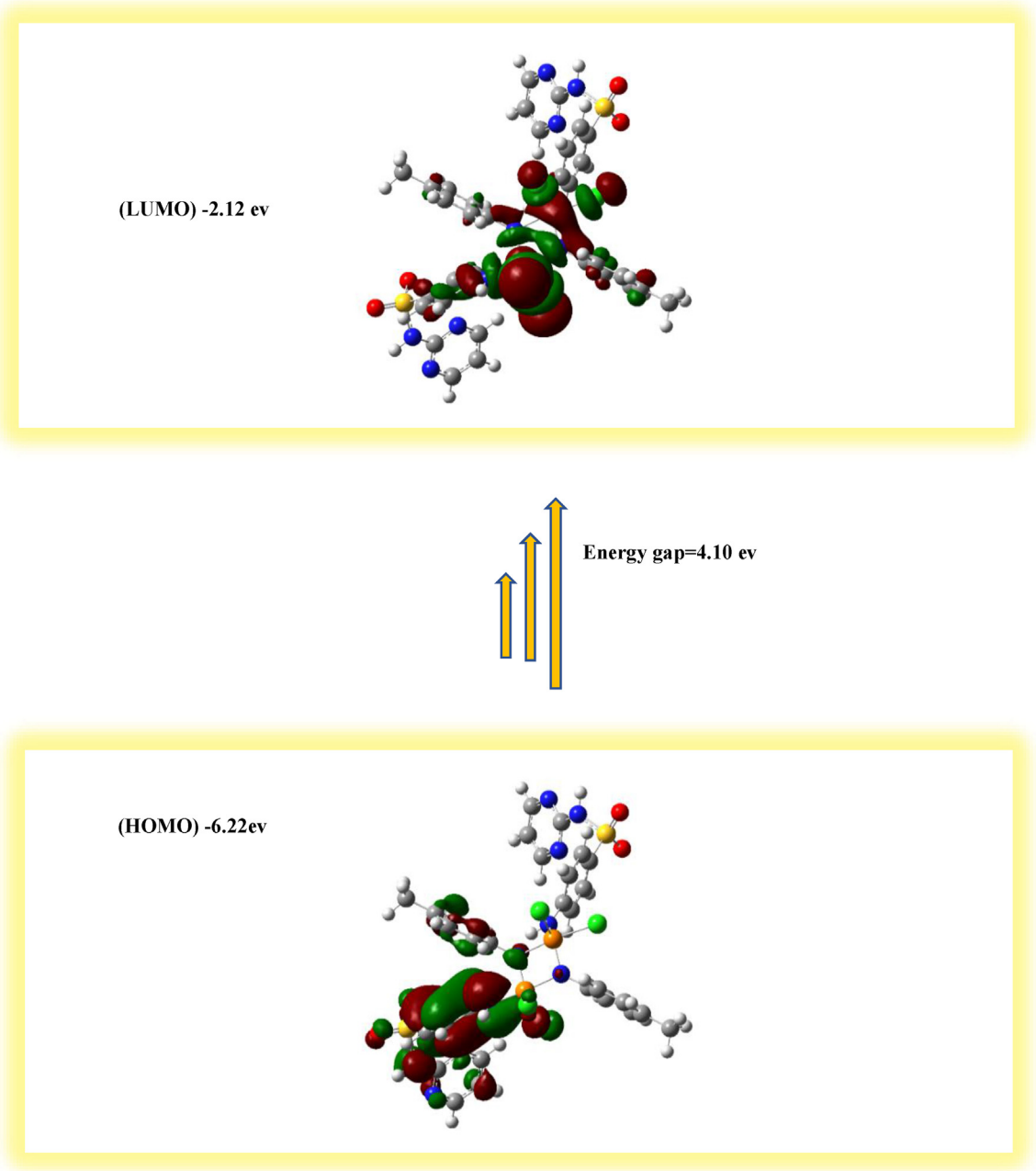

Fig. 8. HOMO–LUMO energy of the H_2L-free ligand.

bipyramidal geometry due to the four-membered ring strain. The exocyclic N–H nitrogen atoms (N_{33} and N_{36}) were slightly trigonal and pyramidal with a dihedral angle of (P_1–N_{33}–H–C_{43}, P_2–N_{36}–H–C_{72}) ~160° Fig. 7.

(1) Molecular orbitals (MOs) are important for investigating molecular reactivity. While HOMO (highest occupied MOs) and LUMO (lowest occupied MO) are prevalent quantum chemical parameters, the HOMO orbital is specifically the highest energy orbital that contains electrons as it functions as an electron donor. The LUMO orbital acted as an electron acceptor because it was the lowest energy orbital that could accept electrons. The energies of HOMO (−6.22 eV) and LUMO (−2.12 eV) were generally negative for the H_2L ligand Fig. 8, which indicates that the molecule was stable. The high HOMO energy indicates that the molecule is a good electron donor [58].

(2) Electrostatic potential (ESP) is a perfect indication and identification of the possible sites representing the electrophilic and nucleophilic attack. Figure 9 shows the electrostatic potential (ESP) distribution of the H_2L ligand obtained by DFT/B3LYP/6–31 g(d,p). In the (ESP) charge distribution, the higher negative value charges are mainly distributed on the electron donor atoms, and the higher positive value charges are

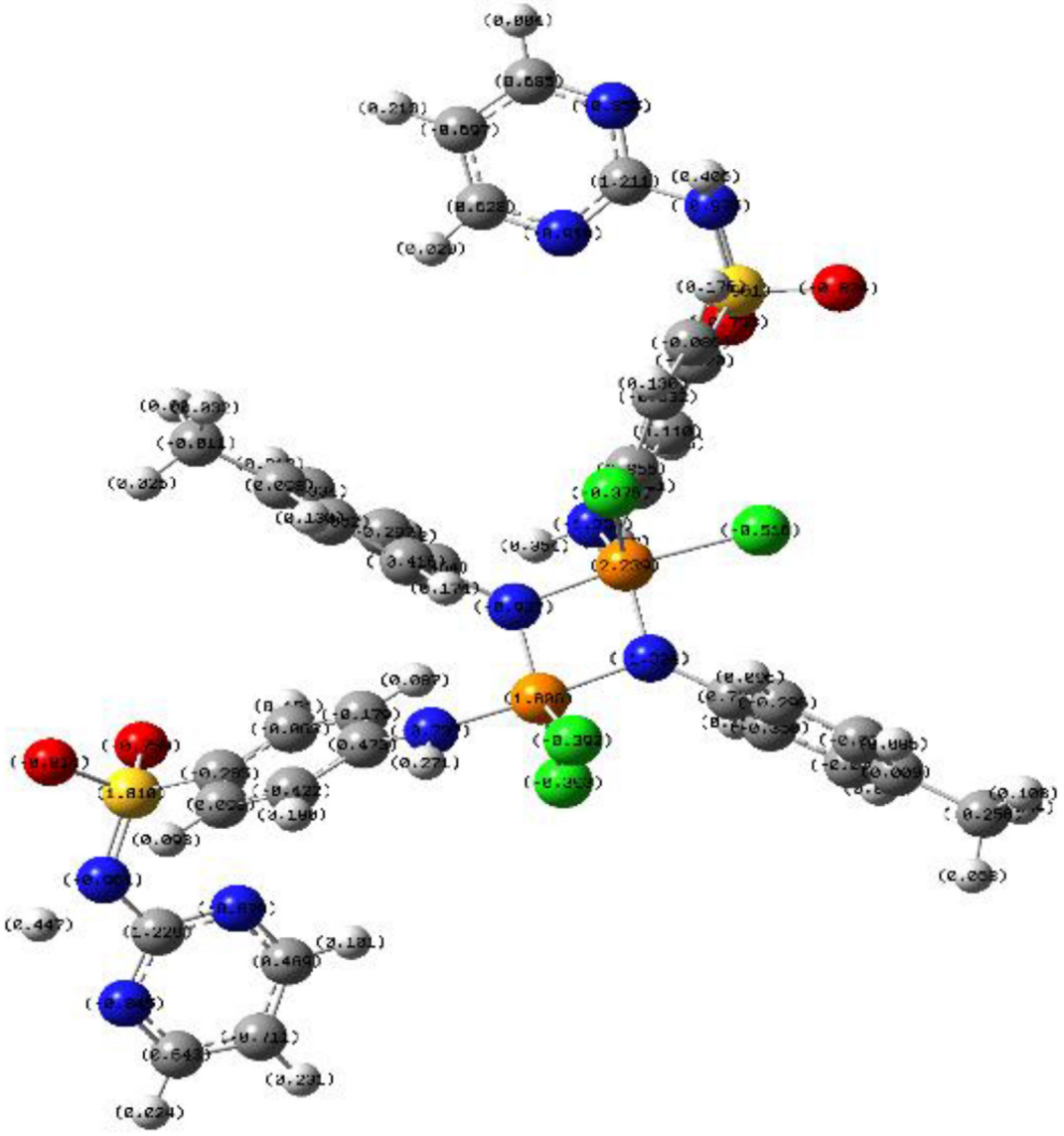

Fig. 9. ESP charge distributions of the H_2L^- free ligand.

mainly distributed on the electron acceptor atoms of the H_2L ligand.

(3) From the data in Table 5, it appeared that the value of ΔE for the H_2L-free ligand was 4.10 eV and the total energy gap (ΔE) was small, indicating the stability of the prepared H_2L-free ligand, proposing it as a good indicator of complexation with adjacent central metal ions owing to its empty *d*-orbital, biological activity, softness, and hence chemically reactive [44,52]. Furthermore, it has been believed that while a ligand should have the capability to receive electrons from the environment, its energy should drop upon doing so, as indicated by the positive electrophilicity index (χ) and the negative chemical potential (Pi) values [52]. In this study, a remarkable change in the bond lengths of the C—N pyrimidine and (C—N, N—S, S—O) sulfonamide groups in zinc and silver complexes confirms the coordination of the H_2L ligand through pyrimidine-N and sulfonamide-O atoms, Table 6. An octahedral geometry was also suggested for the zinc complex from its selected bond length and angle values, showing a remarkable change in bond lengths of the C—N pyrimidine and (C—N, N—S, S—O) sulfonamide groups, which confirms the coordination of the H_2L ligand through pyrimidine-N and sulfonamide-O. The bond angles around the Zn(II) center in the $[(ZnCl_2)_2(H_2L)\ (H_2O)_4]$ complex, Fig. 10 was ~90°, proving that the geometric is octahedral as proposed by the different tools of analyses mentioned previously [58]. The bond angles around the silver complex, Fig. 10 were within range 76.9—124°, corresponding to its distorted tetrahedral geometry [60,73].

(a) The correlation of all the above results for metal complexes gives us information about the suggested structure of metal complexes to be as in Fig. 11.

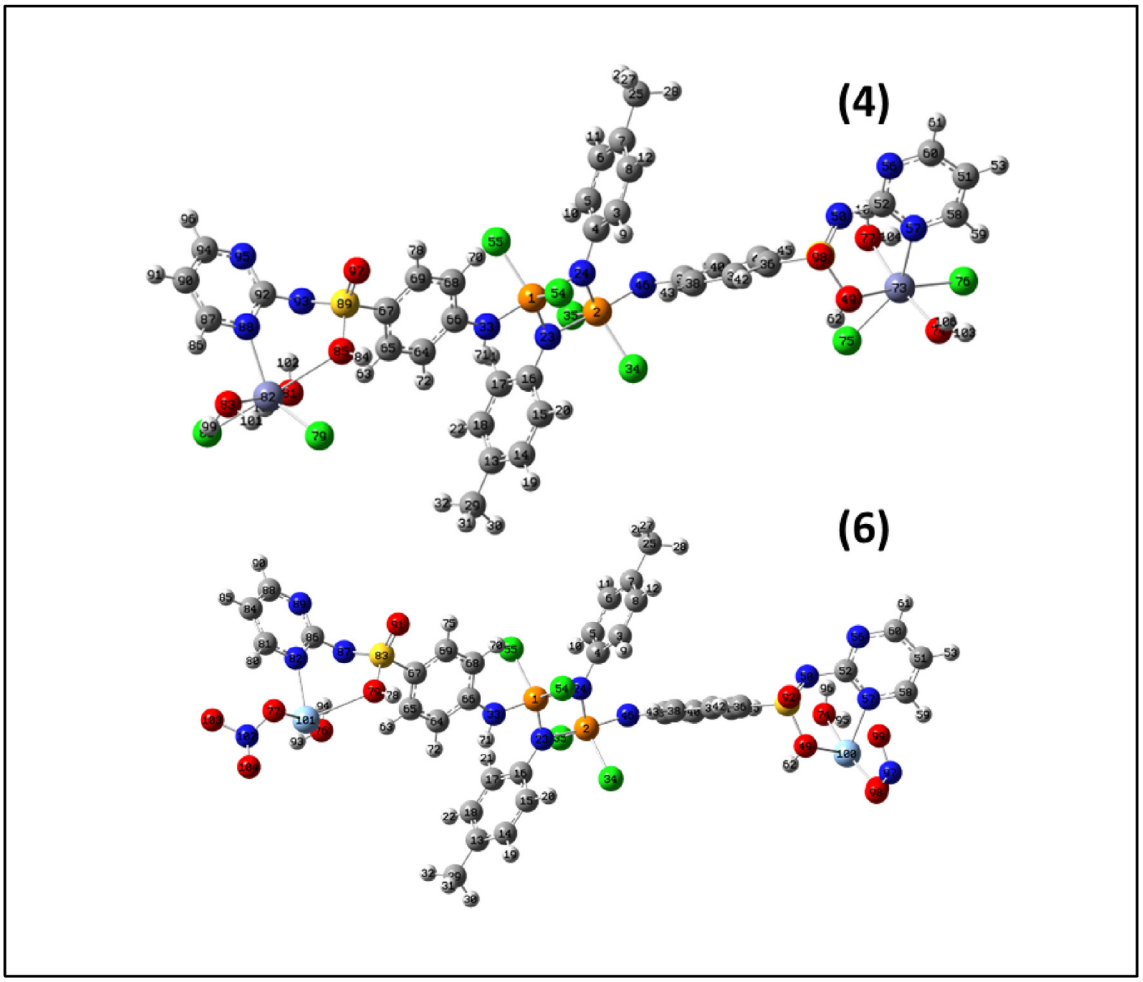

Fig. 10. Optimized structure of $[(ZnCl_2)_2(H_2L)\ (H_2O)_4]$, (4) and $[(AgNO_3)_2(H_2L)\ (H_2O)_2]$, (6) complexes.

3.4. Biological assay

3.4.1. Antimicrobial

The primary goal of synthesizing any antimicrobial agent is to search for novel compounds with an antibacterial activity that does not negatively affect patients [74]. To this end, the antimicrobial activities of all synthesized compounds were screened against microorganisms, two Gram-positive (+ve) bacteria, two Gram-negative (−ve) bacteria, one yeast, and one fungus to assess their potential antimicrobial agents.

Here, we used the agar plate diffusion method [75] to evaluate the antibacterial potential of the freshly synthesized compounds against test microorganisms [75], after which the diameters of the inhibition zones were calculated [76]. Briefly, 100 μL of the test bacteria or fungus was cultured in 10 mL of a new medium until they achieved a count of around 10^8 cells/mL for bacteria or 10^5 cells/mL for fungi.

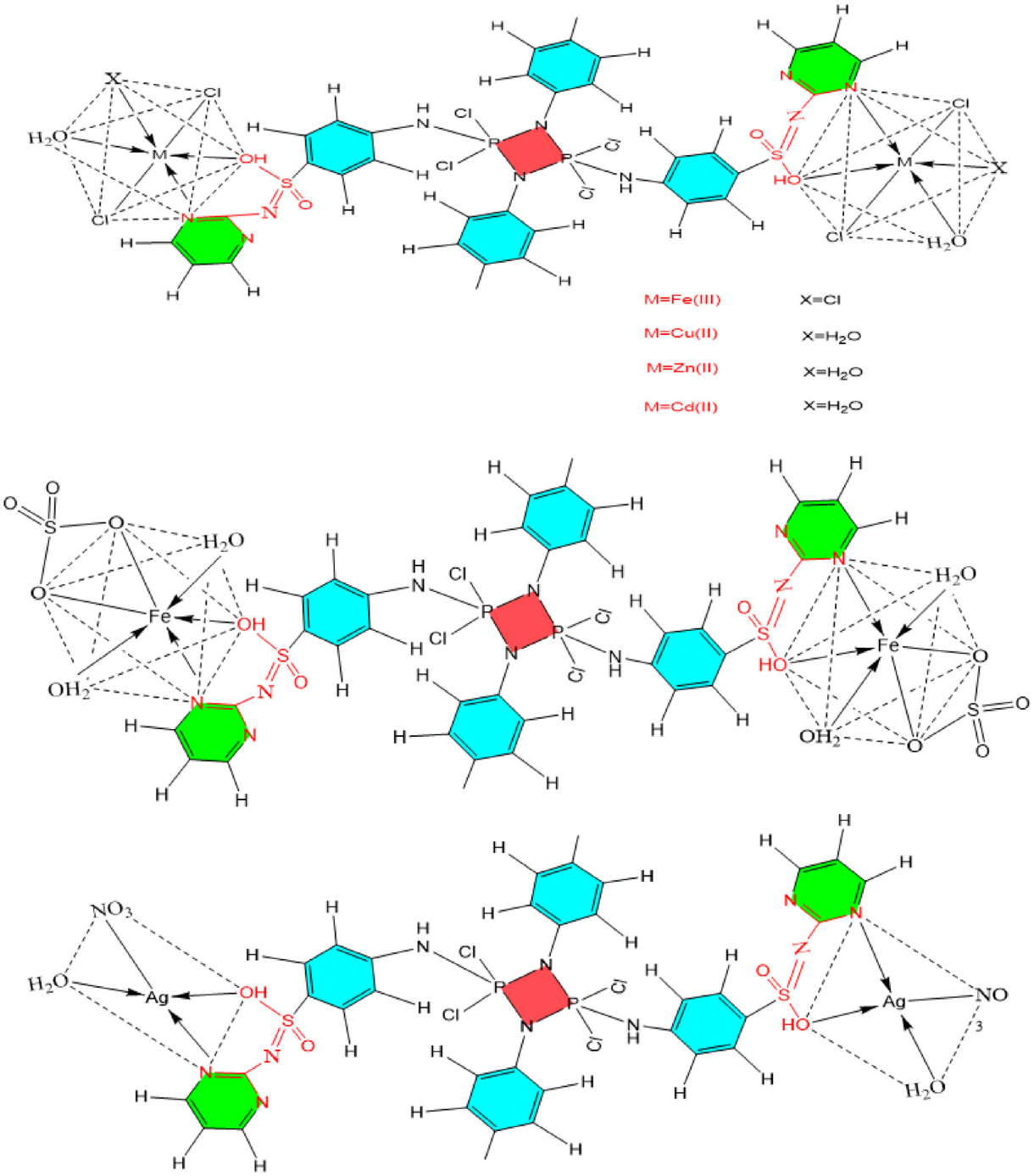

Fig. 11. Suggested structures of metal complexes (1−6).

Table 7. Antimicrobial activity and minimum inhibitory concentration (MIC) for the H2L-free ligand and its complexes (1–6).

Comp. No.	Organism Sample	Gram-positive bacteria				Gram-negative bacteria				Yeasts and Fungi**			
		B. pumilis (MTCC-2296)		*S. faecalis (MTCC − 0459)*		*E. coli* (ATCC -25922)		*E. cloacae* (ATCC-23355)		*C. albicans* (ATCC-10231)		*A. niger (MTCC -1881)*	
		IZ	MIC	IZ	MIC	IZ	MIC	IZ	MIC	IZ	MIC	IZ	MIC
H_2L	H_2L	15I	31.3	21H	7.81	23H	3.91	14I	15.81	14I	62.5	19I	15.63
(1)	$[(FeCl_3)_2(H_2L)\ (H_2O)_2]$	22H	3.91	20H	7.81	24H	15.63	16I	31.3	19I	7.81	12I	62.5
(2)	$[(FeSO_4)_2(H_2L)\ (H_2O)_4]$	17I	1.95	15I	3.91	20H	7.81	23H	7.81	13I	31.3	18I	125
(3)	$[(CuCl_2)_2(H_2L)\ (H_2O)_4]$	19I	15.63	23H	15.63	28H	3.91	20H	31.3	17I	125	13I	62.5
(4)	$[(ZnCl_2)_2(H_2L)\ (H_2O)_4]$	15I	15.63	18I	31.3	27H	7.81	19I	62.5	21H	62.5	24H	31.3
(5)	$[(CdCl_2)_2(H_2L)\ (H_2O)_4]$	23H	3.91	19I	62.5	20H	15.63	19I	7.81	25H	15.63	15I	62.5
(6)	$[(AgNO_3)_2(H_2L)\ (H_2O)_2]$	23H	1.95	19I	7.81	23H	31.3	20H	62.5	17I	62.5	21H	15.63
R.S**		22	≤3	25	≤2	28	≤2	24	≤3	27	≤20	25	≤15

*The test was done using the diffusion agar technique. Inhibition values ≤ 10 (less active). Inhibition values ≤ 20 (moderately active). Inhibition values > 20 (highly active). Not active = 0.
The antibiotic **Penicillin G was used as the standard reference in the case of Gram-positive bacteria; **Ciprofloxacin** was used as the standard reference in the case of Gram-negative bacteria; and **Ketoconazole** was used as the standard reference in the case of yeasts and fungi.

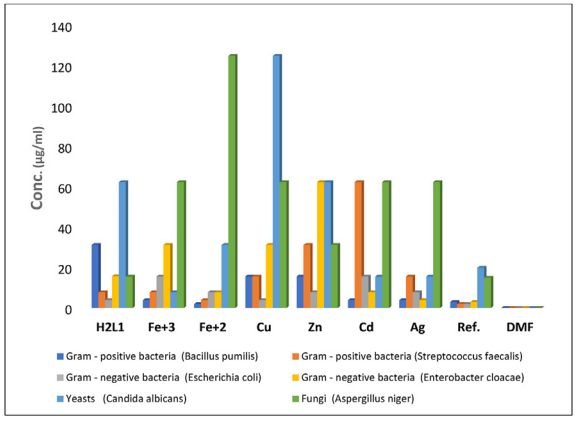

Fig. 12. MIC of H_2L and its metal complexes (1–6).

Then, each well was loaded with 1 ml of each sample (at a concentration of 0.5 mg/ml) after holes with 10-mm diameter were cut into the agar gel, followed by plate incubation for 24 h at 37 °C (for bacteria and yeast) and 72 h at 27 °C (for filamentous fungi). Finally, the growth of the microorganism was observed after incubation using **penicillin G** and **ciprofloxacin** as the standard antibiotics and **ketoconazole** as the standard yeast and fungi control. *In vitro* antimicrobial assessment of the metal complexes and their parent H_2L ligand compared with that of the standard drugs is listed in Table 7. The minimum inhibitory concentration value (MIC µg/ml) results of the synthesized metal complexes and their parent H_2L ligand showed an effective MIC (µg/ml) value compared with the standard antibiotics used. For example, Gram-positive [+ve] bacteria, Fe(II) complex (MIC = 1.95 µg/ml), Ag(I) complex (MIC = 1.95 µg/ml), Fe(III) complex (MIC = 3.91 µg/ml), and Cd(II) complex (MIC = 3.91 µg/ml), with the standard penicillin G (MIC ≤2 µg/ml). However, for Gram-negative [-ve] bacteria, Cu(II) complex (MIC = 3.91 µg/ml) and the standard ciprofloxacin drug (MIC ≤2 µg/ml). For the yeast and fungi Fe(III) complex (MIC = 7.81 µg/ml), Cd(II) complex (MIC = 15.63 µg/ml) and Ag(I) complex (MIC = 15.63 µg/ml) while the standard ketoconazole drug (MIC ≤15 µg/ml) (Table 7 and Fig. 12).

Table 8. Antitumor toxicity of H_2L and its metal complexes (1–6).

Sample	MCF-7 cell line		HCT-116 cell line	
	Inhibition %	(IC_{50} µM)	Inhibition %	(IC_{50} µM)
H_2L	72.86	70.9	70.13	59.14
(1) $[(FeCl_3)_2(H_2L)\ (H_2O)_2]$	85.90	39.0	87.79	21.2
(2) $[(FeSO_4)_2(H_2L)\ (H_2O)_4]$	82.12	42.3	72.77	57.8
(3) $[(CuCl_2)_2(H_2L)\ (H_2O)_4]$	85.13	39.3	83.82	29.7
(4) $[(ZnCl_2)_2(H_2L)\ (H_2O)_4]$	84.20	40.1	74.82	50.2
(5) $[(CdCl_2)_2(H_2L)\ (H_2O)_4]$	88.45	19.57	90.00	13.2
(6) $[(AgNO_3)_2(H_2L)\ (H_2O)_2]$	88.62	15.0	90.24	12.7
Doxorubicin	97.43	2.8	97.57	5.3

(IC_{50} µM): 1–10 (very strong), 11–20 (strong), 21–50 (moderate), 51–100 (noncytotoxic).

3.4.2. In vitro *cytotoxicity*

Cancer is deemed the cruelest disease in humans. So, in this study the cytotoxicity of the H_2L ligand and its metal complexes (1–6) was evaluated against the most common forms of cancer. The growth inhibition of breast (MCF-7) and colon (HCT-116) carcinoma cell lines of the prepared compounds which are presented in Table 8 were compared with the standard anticancer drug, Doxorubicin is used to determine *in vitro* anticancer efficacy. It is obvious from the obtained data that all complexes and their parent H_2L ligand were found to display significant cytotoxic activities by inhibiting the proliferation of MCF-7 and HCT-116 carcinoma cell lines. The data showed that all complexes displayed relatively high inhibition values ranging between (88.62–82.12%) and (90.24–72.77%) for MCF-7 and HCT-116 cancer cell lines, respectively. The effect of different concentrations of the tested compounds on human MCF-7 and HCT-116 cancer cell lines, Fig. 13, showed that the toxicity of the parent H_2L ligand and its complexes was found to be concentration dependent, the cell viability decreased with increasing the concentration of compounds. Then, we calculated the IC_{50} (μM) (value corresponding to the concentration required for a 50% inhibition cell viability) (Table 8, Fig. 14). The data resulted in Table 8 indicated that all complexes displayed respectable IC_{50} values that were superior to that of their parent H_2L ligand. Moreover, in the case of breast cancer MCF-7, complexes indicated IC_{50} values that ranged between 15 and 42.3 μM compared with the IC_{50} value 2.8 μM for the standard drug (Doxorubicin), while in the case of colon cancer HCT-116 cell line, complexes revealed IC_{50} values that ranged between 12.7 and 57.8 μM compared with the IC_{50} value 5.3 μM for the standard drug (Doxorubicin). From the above results, we suggest novel findings toward prospective anticancer medicines against breast and colon cancers. These results might reflect the promising antitumor activity of the newly tested synthetic drugs against MCF-7 and HCT-116 human cancer cell lines.

3.4.3. *Molecular docking studies*

The crystal structures of B92, coupled with a Casp3 protein (PDB ID: 3KJF), were retrieved from the protein data bank. B92 is the ligand that was separated with the Casp3 protein by radiography in the protein data bank and its IUPAC name is [(3S)-3-({[(5S,10aS)-2-{(2S)-4-carboxy-2-[(phenylacetyl) amino]butyl}-1,3-dioxo-2,3,5,7,8,9,10,10a-octahydro-1H- [1,2,4]triazolo [1,2-a]cinnolin-5-yl]carbonyl} amino)-4-oxopentanoic acid]. Then, 3D protonation, in which hydrogen atoms are added to the conventional shape of the enzyme, was used to prepare the molecule for docking. Next, the Moe-Dock, using the triangle matcher placement method and the London dG scoring function, was used to dock the structures of the compounds into protein receptors, after which force field refinement was accomplished on the top five poses per compound. We then redocked B92 with the 3KJF active site to validate the docking process. The results for the interactions of amino acids, affinity by bond

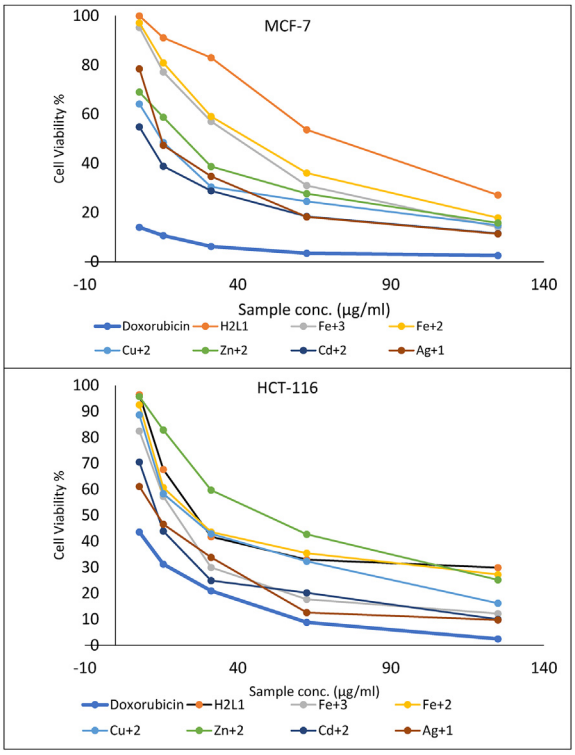

Fig. 13. Cell viability for parent H_2L-free ligand and its metal complexes (1–6) against MCF-7 and HCT-116 cell lines at different concentrations.

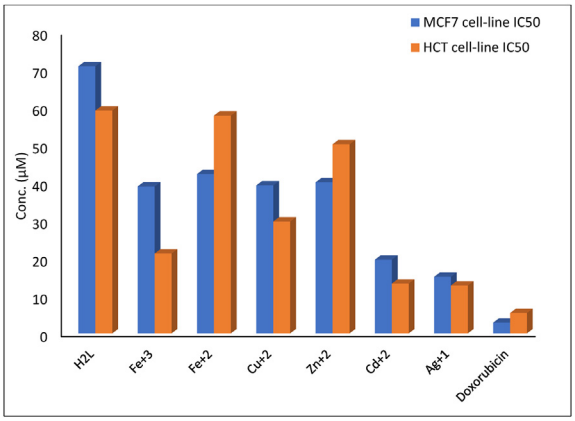

Fig. 14. IC_{50} for parent H_2L-free ligand and its metal complexes (1–6) against MCF-7 and HCT-116 cell lines.

Table 9. Docking interaction data calculations of H_2L, metal complexes of H_2L, and B92 with the active sites of the receptor of Casp3 protein (PDB ID:3KJF).

3KJF						
Comp.	Energy score (S) (Kcal/mol)	Affinity Bond strength (Kcal/mol)	Affinity Bond length (in A° from main residue)	Amino acids	Ligand	Interaction
H_2L	−6.11	−1.3 -2.1 -2.3 -0.9 -2.9 -1.4	3.56 3.36 2.99 3.16 2.99 3.09	Ser 63 His 121 Cys 163 Arg 207 Ser 209 Ser 209	Cl 9 N 45 O 56 N 54 O 70 O 70	H-donor H-donor H-donor H-acceptor H-acceptor H-acceptor
(1) $[(FeCl_3)_2(H_2L)\ (H_2O)_2]$	−6.97	−0.3	3.46	Arg 207	Cl 12	H-donor
(2) $[(FeSO_4)_2(H_2L)\ (H_2O)_4]$	−6.37	−8.5 -3.2	2.98 3.07	Phe 250 Arg 207	N 56 O 79	H-donor H-acceptor
(3) $(CuCl_2)_2(H_2L)\ (H_2O)_4]$	−6.94	−0.8−1.2 -0.8−1.0−2.2−0.7−1.6	3.20 3.14 3.88 3.36 3.14 3.95 4.41	Cys 163 Cys 163 Arg 207 Phe 250 Asn 208 Phe 256 Phe 256	O 16 N 22 Cl 83 Cl 86 N 31C 44 N 88	H-donor H-donor H-donor H-donor H-acceptor H-pi H-pi
(4) $[(ZnCl_2)_2(H_2L)\ (H_2O)_4]$	−6.88	−2.9 -1.3 -3.0	3.00 2.93 3.22	Ser 205 Phe 250 Ser 209	O 5 O 8 N 40	H-donor H-acceptor H-acceptor
(5) $[(CdCl_2)_2(H_2L)\ (H_2O)_4]$	−7.31	−7.6 -0.5 -1.8 -1.6	2.65 3.78 3.37 3.31	Glu 123 Arg 207 Cys 163 Gly 122	O 1 Cl 10 O 16 O 16	H-donor H-donor H-donor H-acceptor
(6) $[(AgNO_3)_2(H_2L)\ (H_2O)_2]$	−10.50	−1.3 -6.3 -0.8 -1.5	3.05 3.42 3.29 3.31	Phe 250 Cys 163 Cys 163 Gly 122	N 6 N 56 O 101 O 101	H-donor H-donor H-donor H-acceptor
B92	−6.58	−2.9 -1.0	2.95 3.79	Tyr 204 Arg 207	O 19 6-ring	H-acceptor Pi-cation

strength in kcal/mol, docking energy score, and lengths of hydrogen bonds in A° are presented in Table 9.

3.4.4. *Docking evaluation against PDB ID: 3KJF*

The data in Table 9 and Fig. 15 show that the co-crystallized B92 exhibited one H-bond with Tyr 204 and a pi-cation contact with the Arg 207 residue.

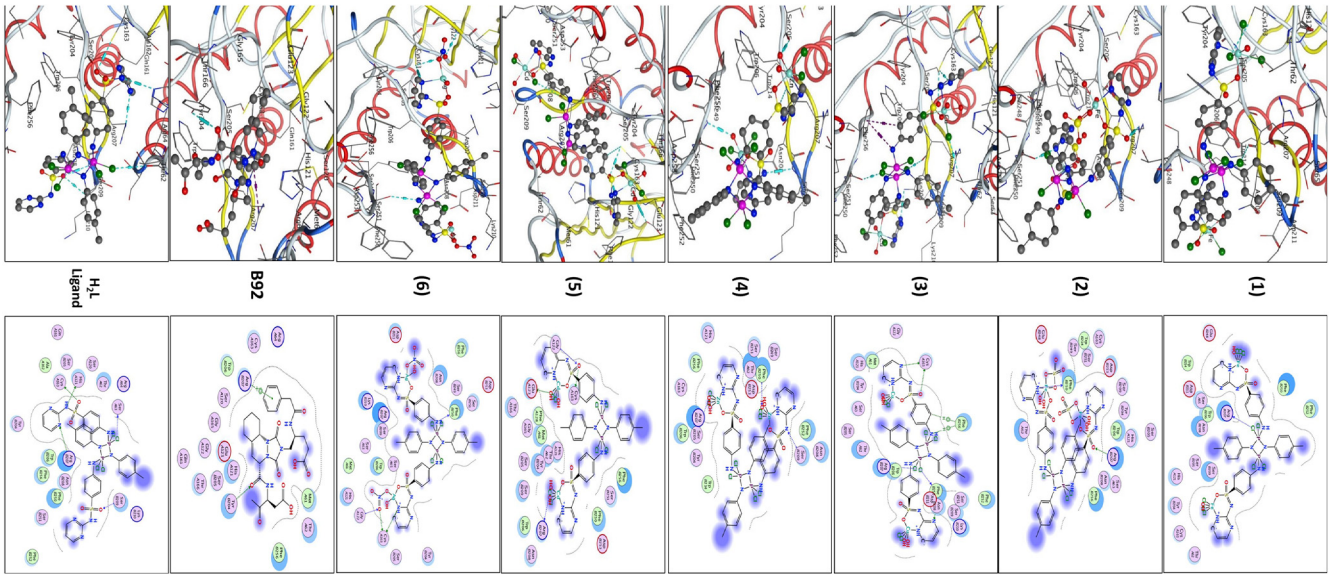

Fig. 15. 2D& 3D interaction of H_2L, its metal complexes (1:6), and B92 in the active site of the receptor of Casp3 protein (PDB ID:3KJF). Hydrogen bonds are displayed in cyan & H-pi-bonds in dark magenta.

Specifically, we observed that the docking energy score of the ligand and its metal complexes, (docking score ranging between −6.11 and −10.50 kcal/mol) were greater than or near that of the co-crystallized B92 (docking score: −6.58 kcal/mol). We also observed that the Ag complex was the metal complex with the best docking score energy (S) = −10.50 kcal/mol, establishing four hydrogen bonds with the Phe 250, Cys 163, Cys 163, and Gly 122 amino acids. This result indicates that the more negative the energy score, the stronger the interaction. Hence, the interaction followed the order $[(AgNO_3)_2(H_2L)\ (H_2O)_2]$>$[(CdCl_2)_2(H_2L)\ (H_2O)_4]$>$[(FeCl_3)_2(H_2L)\ (H_2O)_2]$>$[(CuCl_2)_2(H_2L)\ (H_2O)_4]$>$[(ZnCl_2)_2(H_2L)\ (H_2O)_4]$>$[(FeSO_4)_2(H_2L)\ (H_2O)_4]$>$H_2L$ and agree well with the experimental results of the anticancer activity.

3.5. Conclusion

In this study, we synthesized and characterized a sulfa drug derivative cyclodiazadiphosphetidine-, including its metal complexes (molar ratio (2:1) M:L). As suggested by the conductivity measurements, all complexes showed a non-electrolytic nature. Then, we utilized different spectroscopic, analytical techniques to suggest an exact formula for the prepared compounds and reach a perfect agreement with the spectral studies. An octahedral geometry was adopted for all complexes, and a distorted tetrahedral geometry was suggested for the Ag(I) complex. The geometries have also been optimized using the density functional theory (DFT-B3LYP) methods. Biological studies for determining the antimicrobial activities of complexes and their parent H_2L ligand were carried out against Gram-positive [+ve] bacteria, Gram-negative [−ve] bacteria, yeast, and fungi. The minimum inhibitory concentration value (MIC μg/ml) results of the prepared compounds showed an effective MIC (μg/ml) value compared with the standard antibiotics used. In addition, the cytotoxicity screening showed that all metal complexes had higher antiproliferative activity than their corresponding parent H_2L ligand against two human cancer cell lines. Among all complexes, the Ag(I) complex exhibited more potent activity with the best IC_{50} value. Finally, the parent H_2L ligand and its metal complexes were docked against PDB ID: 3KJF to demonstrate their mode of action as anticancer medicines. Generally, the complexes exerted many interactions and demonstrated high binding to the protein (Casp3). The results indicated that the more negative the energy score, the stronger the interaction.

Conflicts of interest

There are no conflicts to declare.

References

[1] Taha R, Ismail R, Sharaby C, Kamal R, Yahia M. Synthesis and characterization of a symmetrically substituted cyclodiphosph(V)azane ligand and its transition metal complexes for antimicrobial and antitumor investigation. Egypt J Chem 2020; 63:3097–107. https://doi.org/10.21608/ejchem.2020.22722.2349.

[2] Greenwood NN. Earnshaw A chemistry of the elements. 2nd ed.2012. Oxford, UK: Elsevier; 2012.

[3] Al-Mogren MM, Alaghaz ANMA, El-Gogary TM. Spectral and quantum chemical studies on 1,3-bis(N1-4-amino-6-methoxypyrimidinebenzenesulfonamide-2,2,4,4-ethane-1,2-dithiol)-2, 4-dichlorocyclodiphosph(V)azane and its erbium complex. Spectrochim Acta Mol Biomol Spectrosc 2014;118: 481–7. https://doi.org/10.1016/j.saa.2013.09.013.

[4] Wang Z, Fetterly B, Verkade JG. P(MeNMCH2CH2)3N: an effective catalyst for trimethylsilycyanation of aldehydes and ketones. J Organomet Chem 2002;646:161–6. https://doi.org/10.1016/S0022-328X(01)01436-X.

[5] Iranpoor N, Firouzabadi H, Tarassoli A, Fereidoonnezhad M. 1,3,2,4-Diazadiphosphetidines as new P-N ligands for palladium-catalyzed Heck reaction in water. Tetrahedron 2010;66: 2415–21. https://doi.org/10.1016/j.tet.2010.01.099.

[6] El-Sakhawy M, Awad HM, Madkour HMF, El-Ziaty AK, Nassar MA, Mohamed SAA. Preparation and application of organophosphorus dimers as antimicrobial agents for bagasse packaging paper. Cellul Chem Technol 2018;52: 655–62. https://www.cellulosechemtechnol.ro/pdf/CCT7-8(2018)/p.655-662.pdf.

[7] Alaghaz ANMA, Ammar RA, Mohamed HM. Studies on the chelation of cyclodiphosph(V)azane complexes of Co(II), Ni(II), Cu(II), and Pd(II): preparation, characterization, thermal, solid state electrical conductivity, and biological activity studies. Phosphorus, Sulfur, Silicon Relat Elem 2009;184: 2472–90. https://doi.org/10.1080/10426500802505507.

[8] Mohamed TA, Zoghaib WM, Shaaban IA, Farag RS, Alajhaz AEMA. Infrared, 1H and 13C NMR spectra, structural charcterization and DFT calculations of novel adenine-cyclodiphosp(V)azane derivatives. Spectrochim Acta Mol Biomol Spectrosc 2011;83:304–13. https://doi.org/10.1016/j.saa.2011.08.035.

[9] Alaghaz ANMA, Aldulmani SAA. Preparation, Structural characterization and DNA binding/cleavage affinity of new bioactive nano-sized metal (II/IV) complexes with oxazon-Schiff's base ligand. Appl Organomet Chem 2019;33:e5135. https://doi.org/10.1002/aoc.5135.

[10] Briand G. Coordination complexes of bis(amido)cyclodiphosph(III/V and V/V)azane imides and chalcogenides. Coord Chem Rev 2002;233–234:237–54. https://doi.org/10.1016/S0010-8545(02)00033-4.

[11] Chandrasekaran P, Mague JT, Balakrishna MS. Cyclodiphosphazanes with Hemilabile Ponytails: synthesis, transition metal chemistry (Ru(II), Rh(I), Pd(II), Pt(II)), and crystal and molecular structures of mononuclear (Pd(II), Rh(I)) and Bi- and Tetranuclear Rhodium(I) Complexes. Inorg Chem 2005;44:7925–32. https://doi.org/10.1021/ic0509478.

[12] Balakrishna MS. Cyclodiphosphazanes in metal organic frameworks. Phosphorus, sulfur, and silicon and the related elements, vol. 191; 2016. p. 567–71. https://doi.org/10.1080/10426507.2015.1128906.

[13] Healy JD, Shaw RA, Woods M. Phosphorus-nitrogen compounds. Part xliv.1 cyclodiphosph(v)azanes derived from trialkylphosphorothioic triamides. Phosph Sulfur Rel Elem 1978;5:239–43. https://doi.org/10.1080/03086647808069892.

[14] Wheatley N, Kalck P. Structure and reactivity of early–late heterobimetallic complexes. Chem Rev 1999;99:3379–420. https://doi.org/10.1021/cr980325m.

[15] Gray HB, Malmstroem BG. Long-range electron transfer in multisite metalloproteins. Biochemistry 1989;28:7499–505. https://doi.org/10.1021/bi00445a001.
[16] Alaghaz AMA. Studies of some new amino-cyclodiphosphazane complexes of Co(II), Ni(II), and Cu(II). Phosphorus, Sulfur, Silicon Relat Elem 2008;183:2476–89. https://doi.org/10.1080/10426500801964077.
[17] Helm ML, Noll BC, Norman AD. New cleft-containing heterosubstituted Cyclophosphazanes. Inorg Chem 1998;37:4478–9. https://doi.org/10.1021/ic971583p.
[18] Böhmer V. Calixarenes, macrocycles with(almost) unlimited possibilities. Angew Chem Int Ed Engl 1995;34:713–45. https://doi.org/10.1002/anie.199507131.
[19] Cram DJ, Cram JM (Monographs in Supramolecular Chemistry;. Container molecules and their guests, vol. 4. Cambridge: The Royal Society of Chemistry; 1997. p. 1–4. https://doi.org/10.1039/9781847550620.
[20] El-Sentrisy M. Synthesis, Characterization, biological studies of some new phosphorus-drug complexes and their possible uses as anticancer [Ph.D. Thesis]. [Cairo, Egypt]. Girls): Faculty of Science, Al-Azhar University; 2015.
[21] Hamed AA. Synthesis, Structural characterization and biological activity of selected metal complexes of some novel organic ligands [M.Sc. Thesis]. Girls): Faculty of Science, Al-Azhar University; 2017 [Cairo, Egypt].
[22] Aochar RB, Mahale RG, Dhivare RS. Synthesis, physicochemical, morphological, and antimicrobial study of schiff-base ligands metal complexes. J Res Pharmaceut Sci 2022;8:1–6. https://www.researchgate.net/publication/358413368.
[23] Prajapat G, Gupta R, Bhojak N. Thermal, spectroscopic and antimicrobial properties of novel nickel(II) complexes with sulfanilamide and sulfamerazine drugs. Chem Sci Int J 2018;24:1–13. https://doi.org/10.9734/CSJI/2018/44158.
[24] Becke-Goehring M, Leichner L, Scharf B. Über Phosphorstickstoffverbindungen. XXII. Viergliedrige Ringsysteme mit Phosphor und Stickstoff im Ring. ZAAC J Inorg Gen Chem 1966;343:154–64.
[25] Basset J DRC, Jeffery GH, Mendham J. Vogel's textbook of quantitative inorganic analysis. New York: Longmann Group Ltd; 1978. p. 319. 319.
[26] Gohn A. ESR and elementary particle applications. New York: John, Wiley; 1986. https://link.springer.com/book/10.1007/978-94-009-4075-8.
[27] Orio M, Pantazis DA, Neese F. Density functional theory. Photosynth Res 2009;102:443–53. https://doi.org/10.1007/s11120-009-9404-8.
[28] Becke AD. Density-functional exchange-energy approximation with correct asymptotic behavior. Phys Rev 1988;38:3098–100.
[29] Lee C, Yang W, Parr RG. Development of the Colle-Salvetti correlation-energy formula into a functional of the electron density. Phys Rev B 1988;37:785–9.
[30] Hay PJ, Wadt WR. Ab initio effective core potentials for molecular calculations. Potentials for K to Au including the outermost core orbitale. J Chem Phys 1985;82:299–310.
[31] Frisch MJ, Trucks GW, Schlegel HB, Scuseria GE, Robb MA, Cheeseman JR, et al. Gaussian 09, rev. D.01. Wallingford, CT: Gaussian Inc.; 2016.
[32] Rodríguez-Tudela JL, Barchiesi F, Bille J, Chryssanthou E, Cuenca-Estrella M, Denning D, et al. Method for the determination of minimum inhibitory concentration (MIC) by broth dilution of fermentative yeasts. Clin Microbiol Infect 2003;9. https://doi.org/10.1046/j.1469-0691.2003.00789.x. i–viii.
[33] Molecular Operating Environment (MOE). Molecular operating environment (MOE), 2019.01. Scientific Computing & Instrumentation; 2019.
[34] Sharaby CM. Synthesis, spectroscopic, thermal and antimicrobial studies of some novel metal complexes of Schiff base derived from [N1-(4-methoxy-1,2,5-thiadiazol-3-yl)sulfanilamide] and 2-thiophene carboxaldehyde. Spectrochim Acta Mol Biomol Spectrosc 2007;66:1271–8. https://doi.org/10.1016/j.saa.2006.05.030.
[35] El-Gamasy S, Ebrahim S. 4N donor atoms moiety of transition metal complexes of a Schiff base ligand: synthesis, characterization and biological activities study. Egypt J Chem 2021;64:5975–87. https://doi.org/10.21608/EJCHEM.2021.71668.3575.
[36] Silverstein RM, Webster FX, Kiemle D. Spectrometric identification of organic compounds. New York, United States: John Wiley & Sons; 2004.
[37] Huma R, Mahmud T, Awan SJ, Ashraf M, Khan SU, Rasheed H, et al. Thermal and spectroscopic studies of some metal complexes with a new enaminone ligand 3-chloro-4-((4-methoxyphenyl)amino)pent-3-en-2-one and their investigation as anti-urease and cytotoxic potential drugs. Arab J Chem 2022;15:103640. https://doi.org/10.1016/j.arabjc.2021.103640.
[38] Robertson LP, Moodie LWK, Holland DC, Jandér KC, Göransson U. Sulfadiazine masquerading as a natural product from scilla madeirensis (scilloideae). J Nat Prod 2020;83:1305–8. https://doi.org/10.1021/acs.jnatprod.0c00163.
[39] Sharaby CM. Preparation, characterization and biological activity of Fe(III), Fe(II), Co(II), Ni(II), Cu(II), Zn(II), Cd(II) and UO2(II) complexes of new cyclodiphosph(V)azane of sulfaguanidine. Spectrochim Acta Mol Biomol Spectrosc 2005;62:326–34. https://doi.org/10.1016/j.saa.2004.12.047.
[40] Taha R. Synthesis, and studies of metal complexes derived from selected organic ligands containing donor atoms [Ph.D Thesis]. Girls): Al-Azhar University, Faculty of Science; 2014 [Cairo].
[41] Mohamed GG. New Cyclodiphosph(V)azane complexes of Fe(III), Co(II), Ni(II), Cu(II), Zn(II), and UO 2 (II): preparation, characterization, and biological activity studies. Phosp Sulfur Silicon Relat Elem 2005;180:1569–86. https://doi.org/10.1080/104265090884238.
[42] Alaghaz ANMA, Elbohy SAH. New Tetrachlorocyclodiphosph(V)azane complexes of Co(II), Ni(II), and Cu(II): preparation, characterization, solid state electrical conductivity, and biological activity studies. Phosphorus, Sulfur, and Silicon and the Related Elements. 2008. p. 2000–19. https://doi.org/10.1080/10426500701839858.
[43] Sharaby CM, Amine MF, Hamed AA. Synthesis, structure characterization and biological activity of selected metal complexes of sulfonamide Schiff base as a primary ligand and some mixed ligand complexes with glycine as a secondary ligand. J Mol Struct 2017;1134:208–16. https://doi.org/10.1016/j.molstruc.2016.12.070.
[44] Ramadan AM, Bayoumi HA, Elsamra RMI. Synthesis, characterization, biological evaluation, and molecular docking approach of nickel (II) complexes containing O, N-donor chelation pattern of sulfonamide-based Schiff bases. Appl Organomet Chem 2021;35:e6412. https://doi.org/10.1002/aoc.6412.
[45] Salman AA, Abd-ellah IM, El-khazandar AN, El-Wahab ZHA. Studies on cyclodiphosphazanes: some reactions of active-methylene group containing compounds. Phosph Sulfur Rel Elem 1988;40:9–17. https://doi.org/10.1080/03086648808072887.
[46] Mahmoud WH, Mohamed GG, El-Sayed OY. Coordination compounds of some transition metal ions with new Schiff base ligand derived from dibenzoyl methane. Structural characterization, thermal behavior, molecular structure, antimicrobial, anticancer activity and molecular docking studies. Appl Organomet Chem 2018;32:e4051. https://doi.org/10.1002/aoc.4051.
[47] Sharaby CM. Studies of some new cyclodiphosphazane complexes of Fe(III), Fe(II), Co(II), Ni(II), Cu(II), Zn(II) and Cd(II). Synthesis and Reactivity in Inorganic, Metal-Organic. Nano-Metal Chem 2005;35:133–42. https://doi.org/10.1081/SIM-200035687.
[48] Hosny NM, Nawar N, Mostafa SI, Mostafa MM. Spectral characterization of metal complexes derived from glycine (Gly) and 2-acetylpyridine (2-APy). J Mol Struct 2011;1001:62–7. https://doi.org/10.1016/j.molstruc.2011.06.019.

[49] Sharaby CM. Synthesis and characterization of new phosphorus-drugs [ph.D Thesis]. Girls): Al-Azhar University, Faculty of Science; 1992 [Cairo].
[50] Abdul-Hassan MM, NKh Mousa. Antimicrobial activity of new transition metal complexes of sulfamethoxazole on nhibiter by Staphylococcus aureus, Pseudomonas aeruginosa, Salmonella typhi and Escherichia coli. In: AIP conference proceedings; 2020. p. 030037. https://doi.org/10.1063/5.0027486.
[51] Rocha M, Piro OE, Echeverría GA, Pastoriza AC, Sgariglia MA, Soberón JR, et al. Co(II), Ni(II) and Cu(II) ternary complexes with sulfadiazine and dimethylformamide: synthesis, spectroscopic characterization, crystallographic study and antibacterial activity. J Mol Struct 2019;1176:605–13. https://doi.org/10.1016/j.molstruc.2018.09.008.
[52] Mahmoud WH, Deghadi RG, Mohamed GG. Metal complexes of novel Schiff base derived from iron sandwiched organometallic and 4-nitro-1,2-phenylenediamine: synthesis, characterization, DFT studies, antimicrobial activities and molecular docking. Appl Organomet Chem 2018;32:e4289. https://doi.org/10.1002/aoc.4289.
[53] Zayed EM, Mohamed GG, Hindy AMM. Transition metal complexes of novel Schiff base. J Therm Anal Calorim 2015;120:893–903. https://doi.org/10.1007/s10973-014-4061-3.
[54] Afifp TH, el Nawawy MA, el Whab ZH, Mahdy HA. Synthesis and biological studies of some novel cyclodiphosphazanes. Phosp Sulfur Silicon Relat Elem 1998;132:101–8. https://doi.org/10.1080/10426509808036978.
[55] Ejidike IP, Bamigboye MO, Clayton HS. Spectral, in vitro antiradical and antimicrobial assessment of copper complexes containing tridentate Schiff base derived from dihydroxybenzene functionality with diaminoethylene bridge. Spectrosc Lett 2021;54:212–30. https://doi.org/10.1080/00387010.2021.1893191.
[56] Khedr AM, Saad FA. Synthesis, structural characterization, and antimicrobial efficiency of sulfadiazine azo-azomethine dyes and their bi-homonuclear uranyl complexes for chemotherapeutic use. Turk J Chem 2015;39:267–80. https://doi.org/10.3906/kim-1409-21.
[57] Elbohy SAH. Synthesis and electrochemical studies of some metal complexes with phosphorus schiff base ligand. Int J Electrochem Sci 2013;8:12387–401. https://www.researchgate.net/publication/286844258_Synthesis_and_Electrochemical_Studies_of_Some_Metal_Complexes_with_Phosphorus_Schiff_Base_Ligand.
[58] Aljahdali M, El-Sherif AA. Synthesis, characterization, molecular modeling and biological activity of mixed ligand complexes of Cu(II), Ni(II) and Co(II) based on 1,10-phenanthroline and novel thiosemicarbazone. Inorg Chim Acta 2013;407:58–68. https://doi.org/10.1016/j.ica.2013.06.040.
[59] Mahmoud NF, Abbas AA, Mohamed GG. Synthesis, characterization, antimicrobial, and MOE evaluation of nano 1,2,4-triazole-based Schiff base ligand with some d-block metal ions. Appl Organomet Chem 2021;35:e6219. https://doi.org/10.1002/aoc.6219.
[60] Dehno Khalaji A, Shahsavani E, Feizi N, Kucerakova M, Dusek M, Mazandarani R. Silver(I) thiosemicarbazone complex [Ag(catsc)(PPh 3) 2]NO 3 : synthesis, characterization, crystal structure, and antibacterial study. Compt Rendus Chem 2017;20:534–9. https://linkinghub.elsevier.com/retrieve/pii/S1631074816302387.
[61] Njogu EM, Omondi B, Nyamori VO. Silver(I)-pyridinyl Schiff base complexes: synthesis, characterisation and antimicrobial studies. J Mol Struct 2017;1135:118–28. https://doi.org/10.1016/j.molstruc.2017.01.061.
[62] el Tabl A, Abd Wlwahed M, Abd-Elwareth M, Faheem S. Nano metal complexes in cancer therapy, preparation, spectroscopic, characterization and anti-breast cancer activity of new metal complexes of alanine Schiff-base. Egypt J Chem 2021;64:3131–52. https://doi.org/10.21608/ejchem.2021.52415.3082.
[63] Nassar MY, Aly HM, Moustafa ME, Abdelrahman EA. Synthesis, characterization and biological activity of new 3-substitued-4-amino-5-hydrazino-1,2,4-triazole schiff bases and their Cu(II) Complexes: a new approach to CuO nanoparticles for photocatalytic degradation of methylene blue dye. J Inorg Organomet Polym Mater 2017;27:1220–33. https://doi.org/10.1007/s10904-017-0569-x.
[64] Rao NN, kishan E, Gopichand K, Nagaraju R, Ganai AM, Rao PV. Design, synthesis, spectral characterization, DNA binding, photo cleavage and antibacterial studies of transition metal complexes of benzothiazole Schiff base. Chem Data Coll 2020;27:100368. https://doi.org/10.1016/j.cdc.2020.100368.
[65] Nagesh GY, Mruthyunjayaswamy BHM. Synthesis, characterization and biological relevance of some metal (II) complexes with oxygen, nitrogen and oxygen (ONO) donor Schiff base ligand derived from thiazole and 2-hydroxy-1-naphthaldehyde. J Mol Struct 2015;1085:198–206. https://doi.org/10.1016/j.molstruc.2014.12.058.
[66] Mohamed GG, Omar MM, Hindy AM. Metal complexes of Schiff bases: preparation, characterization, and biological activity. Turk J Chem 2006;30:361–82. https://journals.tubitak.gov.tr/chem/vol30/iss3/11.
[67] Kremer E, Facchin G, Estévez E, Alborés P, Baran EJ, Ellena J, et al. Copper complexes with heterocyclic sulfonamides: synthesis, spectroscopic characterization, microbiological and SOD-like activities: crystal structure of [Cu(sulfisoxazole)2(H2O)4]·2H2O. J Inorg Biochem 2006;100:1167–75. https://doi.org/10.1016/j.jinorgbio.2006.01.042.
[68] Stokes SS, Albert R, Buurman ET, Andrews B, Shapiro AB, Green OM, et al. Inhibitors of the acetyltransferase domain of N-acetylglucosamine-1-phosphate-uridylyltransferase/glucosamine-1-phosphate-acetyltransferase (GlmU). Part 2: optimization of physical properties leading to antibacterial aryl sulfonamides. Bioorg Med Chem Lett 2012;22:7019–23. https://doi.org/10.1016/j.bmcl.2012.10.003.
[69] Saad FA, Khedr AM. Greener solid state synthesis of nanosized mono and homo bi-nuclear Ni(II), Co(II), Mn(II), Hg(II), Cd(II) and Zn(II) complexes with new sulfa ligand as a potential antitumour and antimicrobial agents. J Mol Liq 2017;231:572–9. https://doi.org/10.1016/j.molliq.2017.02.046.
[70] Özbek N, Katõrcõoğlu H, Karacan N, Baykal T. Synthesis, characterization and antimicrobial activity of new aliphatic sulfonamide. Bioorg Med Chem 2007;15:5105–9. https://doi.org/10.1016/j.bmc.2007.05.037.
[71] Gangadhararao G, Kumara Swamy KC. Cyclodiphosphazanes as synthetic probes: P-C/P-N bond formation from the reaction with functionalized propargyl alcohols and N-hydroxy substrates. J Chem Sci 2015;127:197–207.
[72] Klare H, Neudörfl JM, Goldfuss B. New hydrogen-bonding organocatalysts: chiral cyclophosphazanes and phosphorus amides as catalysts for asymmetric Michael additions. Beilstein J Org Chem 2014;10:224–36.
[73] Dehno Khalaji A, Shahsavani E, Feizi N, Kučeráková M, Dušek M, Mazandarani R, et al. Ultrasonic-bath-assisted preparation of mononuclear copper(I) thiosemicarbazone complex particles: crystal structure, characterization and antimicrobial activity. Compt Rendus Chem 2017;20:125–31.
[74] Khalil MMH, Ismail EH, Mohamed GG, Zayed EM, Badr A. Synthesis and characterization of a novel schiff base metal complexes and their application in determination of iron in different types of natural water. Open J Inorg Chem 2012;2:13–21. https://doi.org/10.4236/ojic.2012.22003.
[75] Bonev B, Hooper J, Parisot J. Principles of assessing bacterial susceptibility to antibiotics using the agar diffusion method. J Antimicrob Chemother 2008;61:1295–301.
[76] El-Sharief MAMSh, Abbas SY, Zahran MA, Mohamed YA, Ragab A, Ammar YA. New 1,3-diaryl-5-thioxo-imidazolidin-2,4-dione derivatives: synthesis, reactions and evaluation of antibacterial and antifungal activities. Z Naturforsch B Chem Sci 2016;71:875–81. https://doi.org/10.1515/znb-2016-0054.